Surfaces and Interfaces 72 (2025) 107387

Contents lists available at ScienceDirect

Surfaces and Interfaces

journal homepage: www.sciencedirect.com/journal/surfaces-and-interfaces

Effect of sulfide in a 0.2 M NaCl solution on copper and pre-oxidized copper in oxic conditions

Klara Prijatelj, Tadeja Kosec *

Slovenian National Building and Civil Engineering Institute, Dimičeva ulica 12, 1000 Ljubljana, Slovenia

ARTICLE INFO

Keywords:
Copper
Pre-oxidized copper
Chloride and sulfide environment
Electrochemical properties
Surface characterization
Raman
Cyclic voltammetry

ABSTRACT

This study investigated copper and pre-oxidized copper immersed in 0.2 M NaCl solutions containing different concentrations of sulfide ions. In order to investigate the corrosion processes, the corrosion potential and electrochemical impedance at room temperature and at an elevated temperature were measured for 24 h during and after exposure to the chloride solution with different sulfide concentrations in aerated conditions. The surfaces of the pre-oxidized copper were characterized by scanning electron microscopy, energy dispersive X-ray spectroscopy (EDS), a focused ion beam scanning electron microscopy (FIB-SEM), and Raman spectroscopy. It was shown that the concentration of sulfide ions in the chloride environments, in addition to the temperature itself, greatly affect the film formation in oxic conditions. The thickness of the films observed corresponds well to those calculated using cathodic stripping voltammetry. The mechanism of corroding copper in chloride/sulfide system was proposed.

1. Introduction

Copper and many of its alloys have favorable combinations of desirable properties, including high electrical conductivity, wear and corrosion resistance, tensile strength, solderability, and an appealing appearance [1–3]. When exposed to a humid, aerated environment, copper and its alloys spontaneously form copper(I) oxide, Cu_2O, which is insoluble in water and slightly soluble in acid [4–7]. In the presence of aggressive species, and depending on the nature of the environment, further oxidation occurs. The further oxidation of Cu_2O leads to the formation of copper(II) oxide, CuO. CuO nanostructures have been studied to explore their structural, electrochemical and functional properties as they are used for advanced applications such as energy storage, catalysis, biomedical (antibacterial) and environmental application [8–13]. In various environmental conditions, the corrosion rate depends on the aggressiveness of the environment. In an industrial atmosphere, over 20 years of exposure, the corrosion rate of copper is typically under 2.5 μm/year [5,14]. In aerated solutions, such as 0.1 M NaCl, the corrosion rate of copper is between 15 μm/year and 123 μm/year, depending on the microstructural characteristics of the copper [15]. In aerated seawater, the corrosion rate has been shown to be between 25 and 70 μm/year [16,17]. The corrosion rate of copper-based alloys in soil have been shown to be 0.05–4 μm/year for exposure durations of <20 years, tending to decrease with time [18]. An interesting observation of a great number of bronze artifacts from the Bronze Age is that the thickness of the corrosion products was 10–250 μm when the alloy core was present [18].

The corrosion behavior of copper and copper alloys in aqueous media, seawater, and other saline environments has been investigated extensively [19–24]. Corrosion processes lead to the formation of surface films, which can be either protective or non-protective [21]. A crucial role in the formation and properties of the corrosion film in a chloride-containing environment plays chloride ion, with competition between Cl^- and OH^- for surface sites being the first step [23]. Cu_2O is more likely to form at a higher pH, while at higher chloride concentrations the formation of $CuCl_2^-$ is more desirable [23,25]. North and Pryor et al. [22], observed Cu_2O films with traces of atacamite ($Cu_2Cl(OH)_3$) on copper exposed to 3.4 % NaCl. El Warraky et al. [26] found that the CuCl film is less protective than Cu_2O in chloride-containing media. The formation of CuCl on the Cu_2O surface leads to defects that can initiate pitting, so that copper continues to dissolve and Cu_2O continues to grow [25,26]. Other anions such as bicarbonate, nitrate, chloride, and sulfate can also contribute to pitting [26].

The presence of sulfides in chloride media has been studied for more than four decades, particularly concerning copper and copper alloys in seawater polluted with sulfides [20]. The corrosion of copper also occurs

* Corresponding author.
E-mail address: tadeja.kosec@zag.si (T. Kosec).

https://doi.org/10.1016/j.surfin.2025.107387
Received 22 May 2025; Received in revised form 2 August 2025; Accepted 7 August 2025
Available online 8 August 2025

in soil, where copper interacts with sulfide, such as pyrite [27]. Early studies investigated the behavior of copper-nickel alloys in deaerated conditions, with long-term exposure to sulfide pollution found to significantly impact the protective ability of surface oxides in such environments [3,20,28–30]. Macdonald et al. [31] investigated the corrosion of Cu-Ni alloys in dearated sulfide seawater. In deaerated unpolluted seawater, the corrosion rate of copper was low due to hydrogen ion reduction. In deaerated sulfide polluted seawater, corrosion rate increased due to hydrogen ion reduction. Syrett et al. [20] also concluded that the presence of sulfide and oxygen lead to the formation of a thick non-protective, porous cuprous sulfide layer, which interferes with the normal growth of the protective oxide film in unpolluted environment. Similar observations have been made in more recent studies in sulfide-polluted environments [27,32,33]. In a recent study by Li and co-workers [34], the effect of sulfides on the pitting behavior of copper-nickel alloy was investigated in aerated natural seawater and seawater containing sulfides. Sulfides were shown to significantly accelerate the corrosion of these alloys, with the pits more significant than those induced in natural seawater. After 15 days of Cu-Ni alloys being immersed in sulfide-polluted seawater, the corrosion products consisted of Cu_2S, CuS, Cu_2O, CuO, and nickel oxides ($Ni(OH)_2$, NiO, Ni_2O_3) [34].

Al Kharafi et al. [35] investigated intergranular corrosion of copper in sulfide-polluted salt water. The sulfide ions influence the rate and mode of copper dissolution especially when the impurities such as Ni, Ag, Bi, Ta, etc. segregate to the grain-boundary region. This leads to the formation of a weak Cu_2O layer, which breaks quickly under the effect of sulfide ions [35]. In a recent study, the properties of oxide and sulfide corrosion films on copper were investigated using density functional theory (DFT). It was found that Cu_2S forms compact film only on specific facets of Cu. This could help to understand why Cu_2S is rather porous and non-adherent compared to Cu_2O [36].

Some studies have also investigated the atmospheric corrosion of copper in an environment polluted with hydrogen sulfide (H_2S), particularly in relation to the degradation of electronic components and equipment exposed to such conditions [4,37,38]. The corrosion of copper can also occur as a result of exposure to water containing reduced sulfur or from microbiologically induced corrosion mechanisms involving sulfate-reducing bacteria (SRB) [39,40].

With the selection of copper as a corrosion barrier material in the Swedish/Scandinavian concept for nuclear waste disposal, the behavior of copper in saline environments containing varying amounts of sulfides became a primary research focus for many global research groups. A key element of these studies is their relevance to deep geological disposal environments, where the concentration of oxygen is limited and sulfide ions play a dominant role as an oxidizing species.

Oxygen will be trapped during the sealing and will be consumed by various reactions and also by corrosion of the copper canister. It will also be located in the pore space of HCB blocks and backfill material [25,41]. In the Scandinavian concept, sulfide is already present in the groundwater itself, in concentrations of up to 10^{-4} M and $>10^{-6}$ M [25,42]. In the Canadian concept, sulfides are not present in the groundwater composition [41,43,44], but the source of SH^- is the activity of sulfate-reducing bacteria (SRB), which is more evident under anoxic conditions, where there is no trace of oxygen [45,46].

Recently, research has focused on pre-oxidized copper, as cuprite forms on the surface of copper during handling or in the presence of initial oxygen [47–50]. This cuprite layer represents the typical surface condition of copper [4–6]. Studies are now investigating the effects of various sulfide concentrations, the extent of the sulfide attack in different anion environments, and the underlying mechanisms of such attacks [45,51].

Unlike most studies that focus on copper behavior under strictly anoxic conditions, our research explores unlikely but scenarios that may arise during the early evolution of a deep geological repository–such as localized oxygen exposure due to incomplete sealing, microcraks, or transient oxidizing conditions. While such events are not expected under normal engineered condition, they cannot be entirely excluded. By examining the combined effects of sulfide concentration, oxygen availability, and temperature over a defined time frame, this study provides valuable insights into potential deviations from ideal repository conditions.

The depth and intensity of the sulfide attack, as well as the properties of the oxide film, are examined using cyclic voltammetry, open-circuit potential measurements, electrochemical impedance spectroscopy, and various characterization techniques, including OM (optical microscopy), scanning electron microscope (SEM), FIB-SEM (focused ion beam scanning electron microscope), XPS (X-ray photoelectron spectroscopy), and Raman spectroscopy.

2. Materials and methods

2.1. Sample preparation

Copper samples, in the form of discs ($\theta = 15$ mm), were cut from a 2 mm thick Cu sheet (oxygen-free, high thermal conductivity of 99.95 %, cold-rolled and soft-annealed) from Goodfellow, Huntingdon, England, UK. Further details regarding the composition and properties of this copper material can be found in our earlier publication [15]. For the electrochemical measurements, the copper samples were ground with 800–4000 grit SiC paper, polished to a mirror finish using a 1-μm diamond suspension, rinsed with deionized water, and then ultrasonically cleaned in 96 % ethanol for 3 min and air-dried.

Test samples were copper and pre-oxidized copper.

2.2. Test solutions

A borate buffer with a pH value of 10 was used for preparation of pre-oxidized copper and for electroanalytical purposes using cyclic voltammetry. A tetraraborate buffer was prepared by combining 4.77 g of sodium tetraborate decahydrate ($Na_2B_4O_7{\cdot}10H_2O$, assay $\geq$ 99.5 %, Carlo Erba) and 183 mL of 0.1 NaOH (99+ %, LAB Expert) in 1 L of solution.

To study the effect of sulfides on copper corrosion in oxic conditions the following three test solutions were chosen: 0.2 M Cl^-, 0.2 M Cl^- with $5{\cdot}10^{-6}$ M SH^- and 0.2 M Cl^- with $1{\cdot}10^{-4}$ M SH^-.

NaCl ($\geq$ 99.5 %, Fisher Chemical) was used for preparation of 0.2 M chloride solution and sodium sulfide ($Na_2S{\cdot}9H_2O$, 98+ %, Carlo Erba) was used for preparation of sulfide solutions. All chemicals were of p.a. grade.

The pH values of the solutions were measured using a Mettler Toledo pH meter. At room temperature (22 ± 2), the pH of the chloride solution was 6.9, the pH of the chloride solution with a low sulfide concentration ($5{\cdot}10^{-6}$ M SH^-) was 7.1, and the pH of the solution with a high sulfide concentration ($1{\cdot}10^{-4}$ M SH^-) was 9.6. The pH values of the solutions were also measured at 60 °C. The pH of the chloride solution alone was 6.0, the pH of the chloride solution with a low sulfide concentration was 6.4, and the pH of the solution with a high sulfide concentration was 7.9. The accuracy of measuring pH values at 60 °C, however, is affected by the changed activity of the H^+ ions, the reduced stability of the glass electrode, and the effect of temperature on the reference electrode [52].

2.3. Electrochemical measurements

A three-electrode corrosion cell with a volume of 350 cm^3 and a working electrode embedded in a Teflon holder with an exposed electrode area of 0.785 cm^2 were used for the electrochemical experiments. The reference electrode was Ag/AgCl with 3 M KCl (standard reference potential 0.197 V vs SHE) and the counter electrode was a graphite rod. A Gamry 600 potentiostat/galvanostat was used for the electrochemical measurement of corrosion potential (E_{corr}) and for electrochemical impedance spectroscopy (EIS). An Autolab PGSTAT100 (Netherlands,

2011) was used for cyclic voltammetry. All potentials in this paper refer to Ag/AgCl, unless otherwise stated.

Before each electrochemical experiment, the copper electrodes were cathodically cleaned at –1.4 V for 60 s so as to remove any air-formed oxides.

Cyclic voltammetry was performed to investigate the formation mechanism of copper oxides. The voltammograms were recorded from a starting potential of –1.4 V in the anodic direction up to the anodic potential limit, E_a. E_a were 0.0 V, 0.3 V, 0.7 V, and 1 V. The scan rate was 5 mV/s. Cyclic voltammetry was used and terminated at various potentials to confirm the formation of different copper oxides at several different potentials.

After oxidation, the samples were transformed to electrochemical cell containing test electrolyte. The electrochemical tests were conducted at room temperature (22 ± 2 °C) and at an elevated temperature (60 °C) over a period of 24 h.

Corrosion potential was monitored for the duration of the period (24 h). After 24 h of immersion, electrochemical impedance spectroscopy (EIS) was performed over a frequency range of 100 kHz to 1 mHz using a Gamry 600 potentiostat/galvanostat. The AC perturbation amplitude was 10 mV rms and the number of frequency points per decade was 7. EIS data were fitted using Zview (Scribner, Southern Pines, North Carolina, USA) and interpreted based on equivalent electrical circuits. The goodness of fit values was estimated through chi square value.

Cathodic stripping voltammetry (CSV) was used for the cathodic removal of the oxide and sulfide films that formed on the pre-oxidized copper when exposed to the chloride solutions of different sulfide concentrations. Following 24 h immersion in solutions at different temperatures, the pre-oxidized copper samples were rinsed with deionized water, air-dried, and then immediately transferred to an electrochemical cell for the CSV experiments. The CSV experiments were performed in borate solutions with a pH value of 10, from 0 V to –1.5 V, at a scan rate of 1 mV/s. The experiments were performed at room temperature and in an aerated solution.

The thickness (d) of the oxide layer formed on the copper surface after oxidation was calculated using the charge densities (Q), according to Eq. (1). The estimated thickness of the Cu_2O layer on the pre-oxidized samples was 15 nm. The thickness of the corrosion layer after immersing the samples in various sulfide solutions for 24 h was also estimated from the charge densities. The charge densities were obtained through integration of the cathodic peaks recorded in the cathodic stripping voltammograms, as follows

$$d = \frac{QV_m}{nFr} \tag{1}$$

where d is the oxide thickness (nm), Q is the charge density (C/cm^2), V_m is the molar volume of the oxides and sulfides (cm^3/mol), n is the number of exchanger electrons, r is the roughness coefficient ($r = 1$), and F is the Faraday constant (96,485 C/mol) [53,54]. The molar volume of Cu_2O is 23.9 cm^3/mol, the molar volume of CuO is 12.4 cm^3/mol, and the molar volume of Cu_2S is 27.4 cm^3/mol [55].

2.4. Surface characterization

The surface morphology of samples exposed to chloride solutions of different sulfide concentrations at room (22 °C) and elevated (60 °C) temperatures were inspected using a scanning electron microscope (FIB-SEM ZEISS CrossBeam 550 SEM) equipped with an energy dispersive spectrometer EDS (OctaneElite, EDAX, Pleasanton, California, USA). The instrument was operated at 15 kV with the current probe at 2.5 nA. The elemental composition of the corrosion products was investigated using an energy dispersive X-ray spectrometer (EDS, OctaneElite). A FEI Helios Nanolab 600i FEG-SEM with an energy dispersive X-ray spectroscopy (EDS) detector (Aztec Oxford apparatus, SDD detector, WD 4 mm) was used to determine the thickness of the corrosion products formed on the copper surface. The in-situ cross sections were obtained by FIB milling (Ga^+ ions). An acceleration voltage of 2 kV and a current intensity of 50 pA were used for the cross-sectional imaging. With the FIB-SEM, we can examine the cross-section of the sample and make precise milling and deposits in the nanometer range, but it can also damage or alter the surfaces of the samples.

Raman spectroscopy is a non-destructive technique that provides chemical information on surface composition without requiring vacuum or sample preparation. Corrosion products were analyzed using a Horiba Jobin Yvon LabRAM HR800 Raman spectrometer coupled with an Olympus BXFM optical microscope was used to obtain Raman spectra using a 633 nm laser excitation line, a 100× objective lens, and a 600 grooves/mm grating. The spectra presented include baseline correction.

XPS is surface sensitive technique and is used for the analysis of thin films, oxides and coatings (5–10 nm in depth). XPS can provide quantitative analysis including the chemical composition of the surface. XPS measurements were performed using a Supra+ instrument (Kratos, Manchester, UK) equipped with an Al Kα source, a monochromator, and a charge neutralizer. The take-off angle of the analysis was 90° The binding energy (EB) scale was corrected using the C—C/C—H peak in the C 1 s spectrum at 284.8 eV. The data were acquired and processed using ESCApe 1.4 software (Kratos, Manchester, UK). The pass energy values used to acquire high-resolution (HR) were 40 eV and 160 eV. The Shirley background subtraction algorithm was used [56].

3. Results

3.1. Cyclic voltammetry of copper

Cyclic voltammetry (CV) was performed in a borate buffer (pH 10) to study the oxidation and reduction processes of copper. As described in the literature [54,57], the results from cyclic voltammetry are not identical, due to differences in the surface preparation, contamination, and the corrosion media used. The potential of each voltammogram was reversed at a different potential, as shown in Fig. 1. During the CV scan in the positive direction to the anodic potential limit, $E_a = 0$ V, the first anodic peak, A1, was reached at a potential of –0.19 V. The anodic peak was assigned to the formation of a copper(I) oxide, Cu_2O, which occurs according to Equation 2 [54].

$$2Cu + H_2O = Cu_2O + 2H^+ + 2e^- \tag{2}$$

The reduction scan showed the cathodic peak, C1, at a potential of –0.5 V. It is assigned to the reduction of copper(I) oxide to copper, as shown in Eq. (3) [53,54].

$$Cu_2O + 2H^+ + 2e^- = 2Cu + H_2O \tag{3}$$

Pushing the anodic potential limit to $E_a = 0.3$ V, the second peak, A2, is observed at a potential of –0.03 V. In a borate buffer, the peak A2 oxidizes copper(I) oxide to a copper(II) oxide film. The CuO film is formed according to Eq. (4) [54].

$$Cu_2O + H_2O = 2CuO + 2H^+ + 2e^- \tag{4}$$

Other authors have attributed the second oxidation peak in alkaline solutions (NaOH, KOH) to the formation of a complex hydrous(II) oxide film [58–60]. According to Seo [61], the average composition of the outer layer could be represented as $CuO_x(OH)_{2-2x}$, where x varies in the range of $x = 0 - 1$. This corresponds to the range of composition of Cu $(OH)_2$ to CuO [61].

At higher reverse positive potentials, the second peak, C2, is observed in the negative scans at a potential of –0.17 V, which is attributed to the reduction of the outer layer, i.e., the reduction of copper(II) oxide to copper(I) oxide, as shown in Equation 5 [53].

$$2CuO + 2H^+ + 2e^- = Cu_2O + H_2O \tag{5}$$

Fig. 1a shows that the formation of the anodic peaks (A1 and A2) in a

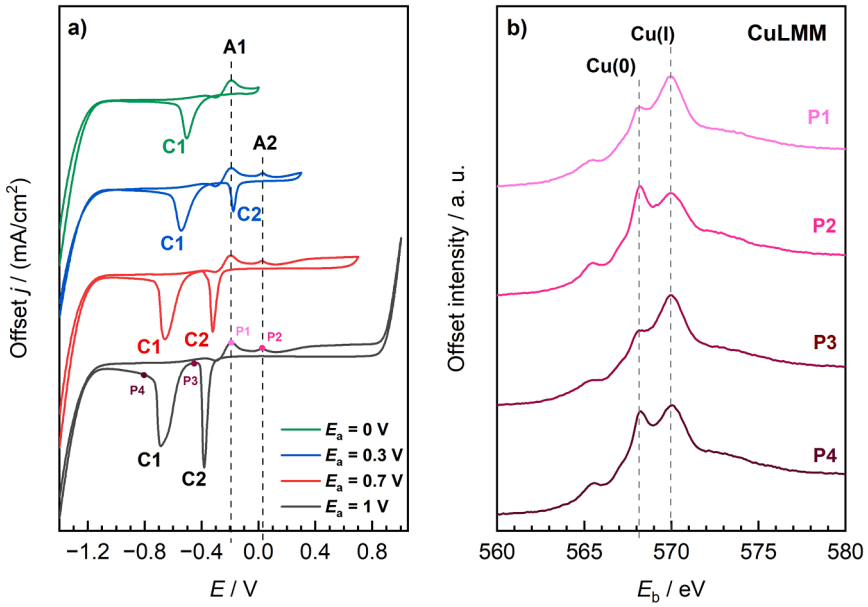

Fig. 1. a) Cyclic voltammograms recorded for copper in a borate buffer (pH 10) with progressively increasing E_a potential, ν = 5 mV/s; b) XPS-induced Auger CuLMM on a copper sample at different oxidation and reduction states (P1, P2, P3, and P4).

positive scan always occur at the same potential. The anodic peak A1 appears at a potential of –0.19 V, while the anodic peak A2 appears at a potential of 0.03 V. The reduction (cathodic) peaks in the negative parts of the CV, however, behave differently. At a higher positive reverse potential, the reverse potential significantly influences the shape and position of the cathodic peaks. The cathodic peak moves towards a more negative potential and the height of the cathodic peak increases, indicating that more copper(I) oxide and copper(II) oxide have formed on the copper surface. This can be most clearly observed between the CVs at E_a values of 0.3 V and 1 V (see Fig. 1a).

In order to prove the formation and reduction of different copper oxides, XPS CuLMM spectra were measured at different stages of the oxidation and reduction processes (Fig. 1b). The first spectrum, P1, represents a copper sample where the CV scan was stopped at the A1 peak for 2 h, which represents the oxidation of Cu to Cu_2O. The thickness (d) of the oxide layer was calculated from the XPS CuLMM spectra and integration of the intensities of the individual species, using Eq. (6) [62],

$$\frac{I_{ox}}{I_m} = \left(\frac{D_{OX}\lambda_{OX}}{D_m\lambda_m}\right)\left[exp^{\frac{d}{\lambda_{ox}cos\Theta}} - 1\right] \quad (6)$$

where D denotes the atomic density, λ is the electron inelastic free path, and Θ is the takeoff angle. The following values were used for the calculations: $D_{Cu} = 0.14$, $D_{Cu2O} = 0.042$, $\lambda_{Cu} = 1.63$ nm, $\lambda_{Cu2O} = 2.91$ nm, and the takeoff angle, Θ, was 90 °

The thickness of the Cu_2O oxide film formed on the copper at the peak A1 was 3.70 nm. A second XPS spectrum was recorded at the peak A2 (area P2), which represents the oxidation of Cu_2O to CuO. The thickness of the Cu_2O layer was 2.95 nm, indicating the oxidation processes. After the first reduction process of CuO to Cu_2O, the XPS spectrum was recorded again (P3 in Fig. 1b). The calculated thickness of the Cu_2O at position P3 was 3.81 nm. This indicated the reduction of CuO to Cu_2O at the cathodic reduction peak at –0.4 V, since the thickness of Cu_2O increased again. The last CuLMM spectrum (P4) was obtained after the second reduction process at C1, where the reduction of Cu_2O to Cu is expected. The thickness of the Cu_2O after the reduction was 3.16 nm, indicating only the partial reduction of Cu_2O.

XPS analysis showed that the oxidation of Cu to Cu_2O at P1 (E = –0.19 V) was consistent with previous findings in a tetraborate buffer [54] and 0.1 M NaOH [45,47]. $Cu(OH)_2$ at P2 was excluded on the basis of the cathodic stripping voltammetry, which revealed two cathodic peaks in a tetraborate buffer, as previously reported [54] and by our results presented in Fig. 1a. In contrast to recent reports on reduction species [45], our results confirm that the cathodic peak, C1, at –0.75 V (E_a = 1 V) corresponds to the reduction of Cu_2O, whereas C2, at –0.4 V, indicates the reduction of CuO. This was also noted by Su [63] in a literature review on the cathodic reduction of copper. The reduction of Cu_2O at –0.5 V (vs. SCE) has also been confirmed previously on naturally grown oxide films on copper in air or in a 0.5 M NaCl solution [64].

3.2. Electrochemical properties of the copper and pre-oxidized copper samples immersed in 0.2 M cl^- solutions with the addition of either $5{\cdot}10^{-6}$ M SH^- or $1{\cdot}10^{-4}$ M SH^-

a) Corrosion potential measurements

The evolution of the corrosion potential of copper and pre-oxidized copper immersed for 24 h in different aqueous solutions at room (22 °C) and elevated (60 °C) temperatures is shown in Fig. 2.

At 22 °C, the corrosion potential, E_{corr}, of copper (Fig. 2a) in the chloride solution (0.2 M Cl^-) and in the solution with a low sulfide concentration (0.2 M Cl^- + $5{\cdot}10^{-6}$ M SH^-) initially dropped to slightly more negative values in the first 2 h, then it increased and remained constant at –0.18 V during the period of immersion. In the solution with the highest sulfide concentration (0.2 M Cl^- + $1{\cdot}10^{-4}$ M SH^-), E_{corr} increased rapidly to more positive values within one hour (up to –0.12 V), but then also decreased rapidly. After 8 h of immersion, a second drop in potential was observed, then E_{corr} slowly stabilized at a value of –0.184 V.

Compared to the exposure at 22 °C, at elevated temperatures (60 °C), Fig. 2b, the corrosion potential values for copper shifted to more negative values within one hour, from –0.17 V to approximately –0.22 V, in all three different solutions. Then E_{corr} began to increase throughout the remainder of the immersion period. The largest increase in potential was observed in the solution with a low sulfide concentration, which reached a final E_{corr} value of –0.191 V after 24 h of immersion. When copper was immersed in only the chloride solution, the corrosion potential initially decreased slightly and then remained constant. In the solution with the highest sulfide concentration, the E_{corr} increased initially, but then slowly decreased over time. At the end of immersion, the E_{corr} value was the most negative (E_{corr}= –0.218 V). In general, the behavior of copper

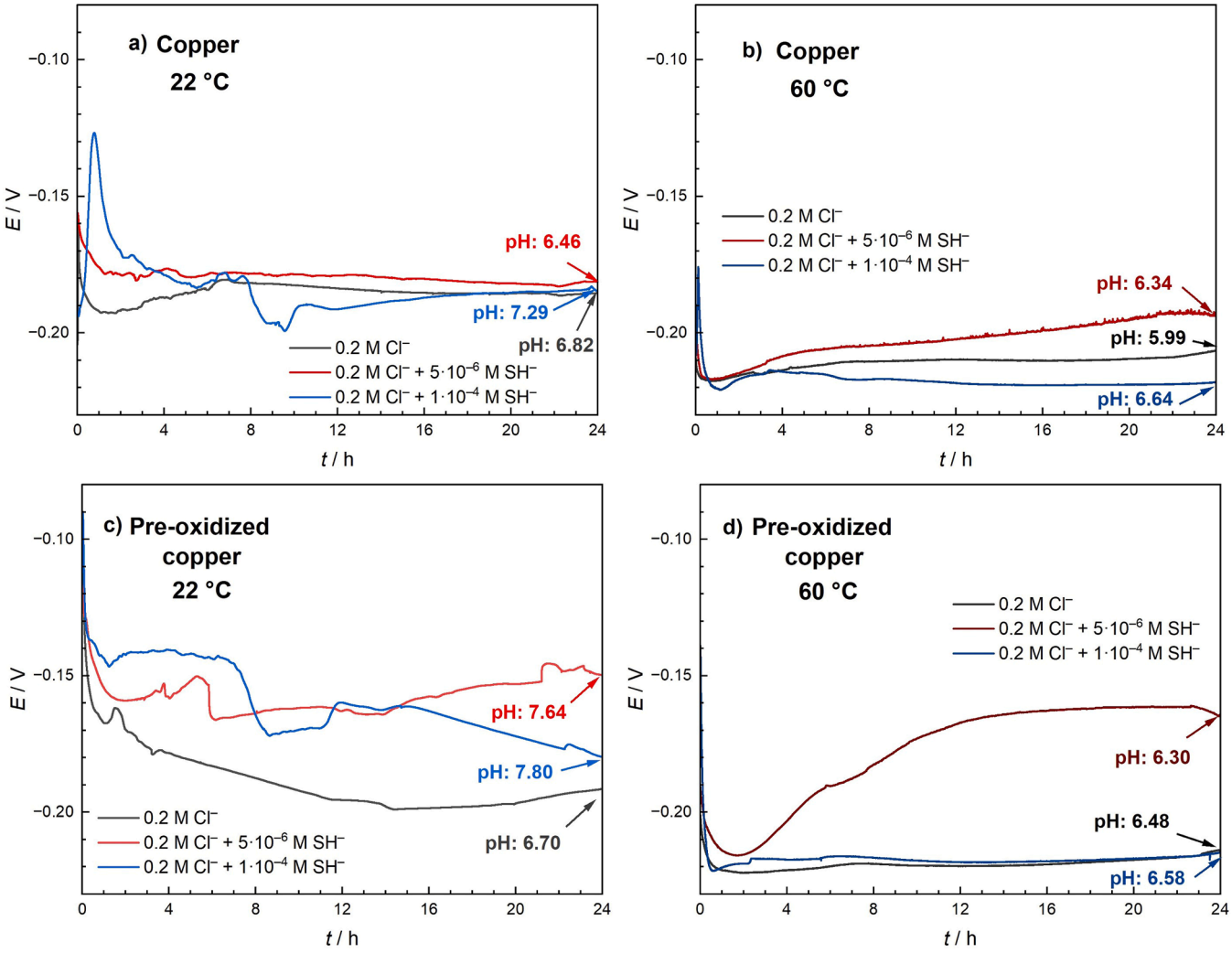

Fig. 2. Evolution of E_{corr} for the copper (a,b) and pre-oxidized copper (c,d) immersed in 0.2 M Cl^-, 0.2 M Cl^- + 5·10^{-6} M SH^-, and 0.2 M Cl^- + 1·10^{-4} M SH^- at 22 °C and 60 °C.

was observed to be similar at both temperatures.

Fig. 2c and 2d shows the evolution of corrosion potential for the pre-oxidized copper immersed in different solutions at room and elevated temperatures.

The first observation was that the E_{corr} values started at more positive values (between –0.09 V and –0.13 V) than when the copper was immersed in the same solutions at room temperature. This can be attributed to the presence of a protective layer of Cu_2O on the surface. At room temperature (22 °C), Fig. 2c, the corrosion potential, E_{corr}, decreased with time in the chloride solution, reaching a final value of –0.191 V after 24 h. In the solution with a low sulfide concentration (5·10^{-6} M SH^-), the E_{corr} value initially decreased, then started to increase after 14 h, reaching a final E_{corr} value of about –0.15 V at the end of the period of immersion. In the solution with the highest sulfide concentration (1·10^{-4} M SH^-), no rapid increase in potential was observed, in contrast to the copper in the same solution (Fig. 2a), but the second drop in E_{corr} occurred at almost the same time, after 8 h of immersion. Over time, E_{corr} continued to decrease slightly, eventually reaching a value of –0.179 V.

At 60 °C (Fig. 2d), the E_{corr} values dropped rapidly in all three solutions to a value of –0.22 V, similar to that observed for the copper immersed at the same temperature (Fig. 2b). In the chloride solution, the E_{corr} value remained almost constant throughout the entire period of immersion, at an E_{corr} value of –0.214 V. The highest increase in corrosion potential was observed for the pre-oxidized copper immersed in the solution with a low sulfide concentration. The E_{corr} value increased from –0.22 V to –0.15 V and then remained constant until the end of the exposure (E_{corr} = –0.164 V). In the solution with a high sulfide concentration, the E_{corr} behaved similarly to the copper (Fig. 2b) in the chloride solution, with the open circuit potential having a similar value (E_{corr} = –0.215 V).

The pH was measured at the end of the period of immersion so as to detect any chemical changes in the solutions, as indicated in Fig. 2. The pH was similar in all of the solutions, with the exception of the high sulfide concentration solutions, where the pH value decreased more significantly from the initial pH of the freshly prepared solutions. The reported decrease of solution pH is mainly caused by the oxidation of sulfide by oxygen in aerated solution. SH^- is unstable and can be converted via the intermediates SO_3^{2-}, $S_2O_3^{2-}$, to SO_4^{2-} where elemental S and polysulphides (S_2^{2-}) are also possible products [65]. The half-life of sulfide in aerated seawater has been reported to be around 17 min [66,67], with the bisulfide ion (HS^-) predominating at pH 7–12. This suggests that under the experimental conditions tested in 0.2 M Cl^- solutions with the addition of 1·10^{-4} M SH^-, both reaction pathways, the direct formation of Cu_2S via reaction between HS^- and copper and the oxidation of unconsumed sulfide occurred since the decrease of pH was observed.

Previous studies reported a slight decrease in the potential of about 40 mV with the addition of sulfide, when measured over a shorter period

of 40 min [3]. Similarly, in previous studies of Cu-Ni alloys exposed to aerated, sulfide-polluted seawater for 24 h, a reduction in the corrosion potential of about 20 mV was observed after 8 h in a heavily sulfide-polluted saline solution [58].

b) Electrochemical impedance spectroscopic measurements

Electrochemical impedance spectroscopy studies after 24 h immersion in various chloride solutions with different sulfide concentrations allowed observation of the properties of the surface films on the copper and pre-oxidized copper.

The Nyquist and Bode plots for the copper in chloride solutions of different sulfide concentrations at both 22 °C and at 60 °C are shown in Fig. 3. The measurements were carried out after the copper samples had been immersed in the different solutions for 24 h. The lines show the fits to the equivalent circuits. The Bode diagram shows two clearly resolved time constants at high to mid and low frequencies. A diffusion response at low frequencies is clearly observed in the Nyquist diagrams in all three solutions. In the chloride solution without sulfide, the total impedance at the lowest measured frequency ($\nu = 1$ mHz) was of the order of 17.0 kΩ cm^2. In the chloride solution with a low sulfide concentration ($5{\cdot}10^{-6}$ M SH$^-$), the total impedance increased ($|Z| = 22.0$ kΩ cm^2), whereas the total impedance in the solution with a high sulfide concentration ($1{\cdot}10^{-4}$ M SH$^-$) was 15.8 kΩ cm^2.

Similar behavior was observed at 60 °C. In the chloride solution without added sulfide, the total impedance at a low frequency was of the order of 3.17 kΩ cm^2. In the chloride solution with a low sulfide concentration the total impedance increased to 7.82 kΩ cm^2, but at a high sulfide concentration the total impedance decreased ($|Z| = 2.95$ kΩ cm^2). Two dinstinct semicircles representing two time constants in the system are observed in the Nyquist diagram. The high-frequency semicircle represents the charge transfer resistance or double layer

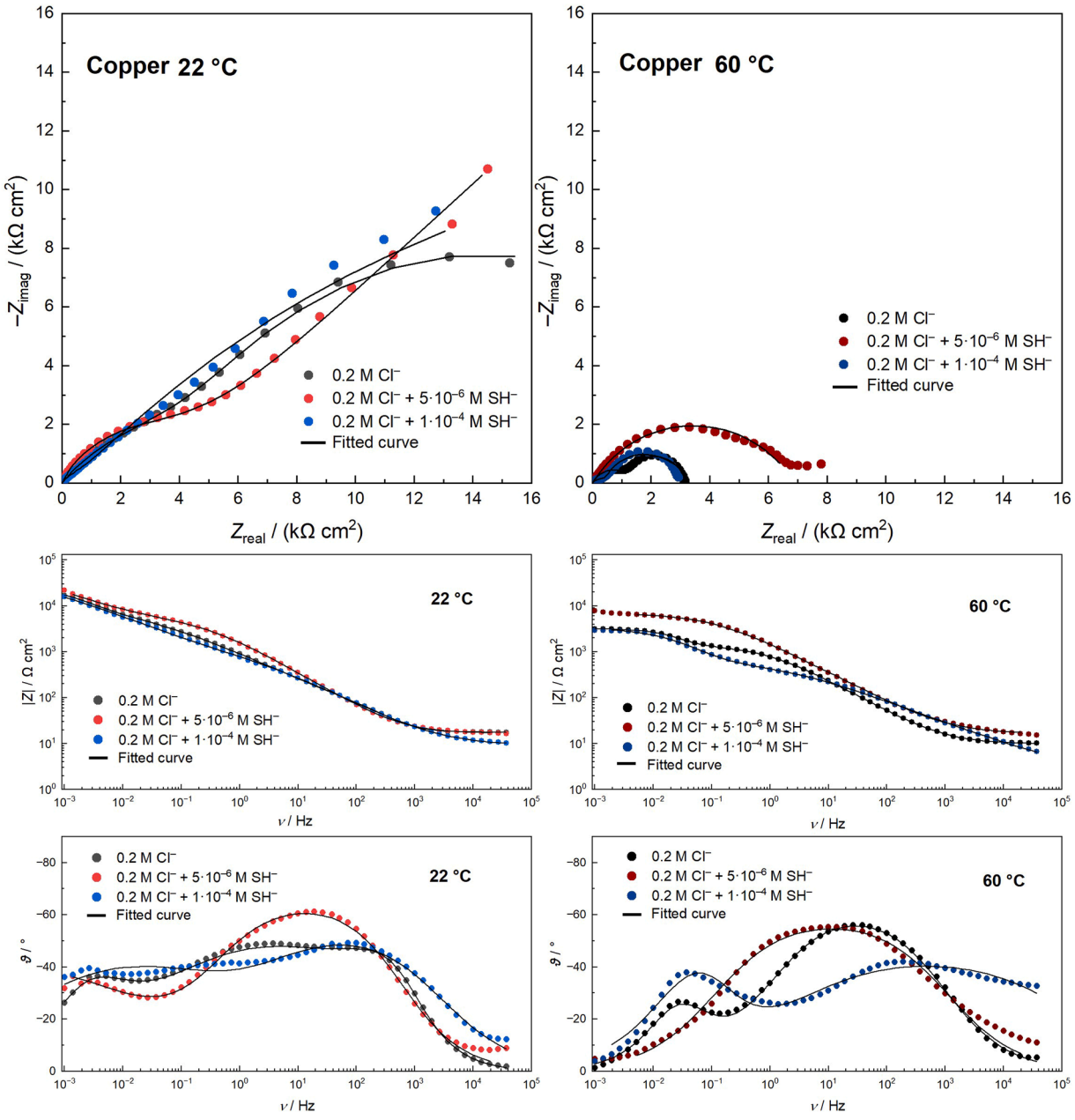

Fig. 3. Nyquist and Bode diagrams of the copper after 24 h immersion in three different solutions (0.2 M Cl$^-$, 0.2 M Cl$^-$ + 5·10^{-6} M SH$^-$, and 0.2 M Cl$^-$ + 1·10^{-4} M SH$^-$) at 22 °C and 60 °C.

capacitance, while the low-frequency semicircle describes the diffusion processes, most probably within the oxide layer.

Fig. 4 shows EIS spectra recorded on the pre-oxidized copper samples in chloride solutions of different sulfide concentrations at 22 °C and at 60 °C after 24 h of immersion.

At 22 °C, the Nyquist and Bode plots for the pre-oxidized copper in different solutions show two capacitive loops, indicating two well-separated processes at high and low frequencies. In the chloride solution, the total impedance at the lowest frequency ($\nu = 1$ mHz) was of the order of 18.7 kΩ cm^2, which is 10 % higher than when the copper was immersed in the chloride solution. The higher total impedance can be attributed to the presence of an oxide layer (Cu_2O). In the chloride solution with a low sulfide concentration, the total impedance at 10 mHz (the measurement was aborted due to a system error) was 13.1 kΩ cm^2, while in the solution with a high sulfide concentration the total impedance at a frequency of 1 mHz was 13.7 kΩ cm^2.

At 60 °C, two well-separated semicircles can be observed in the Nyquist diagram. Similar to before, these indicate the presence of several electrochemical processes that contribute to the overall impedance response while the pre-oxidized copper is immersed in different solutions. The total impedance at the lowest frequency ($\nu = 1$ mHz) was smaller in the chloride solution, at 3.38 kΩ cm^2. In the solution with a low sulfide concentration, the total impedance was higher ($|Z| = 7.82$ kΩ cm^2), while in the solution with a high sulfide concentration the total impedance was 3.44 kΩ cm^2. At 60 °C, the behaviour of the pre-oxidized copper was very similar to that of the copper in 0.2 M Cl$^-$.

The impedance spectra were analysed by fitting the experimental data to the electrical equivalent electrical circuits, as shown in Fig. 5. The symbols in Figs. 3 and 4 represent the experimental data and the solid lines depict the fitted curves. The fitted parameter values are summarized in Tables 1 and 2.

Impedance spectra could be fitted with an equivalent circuit using

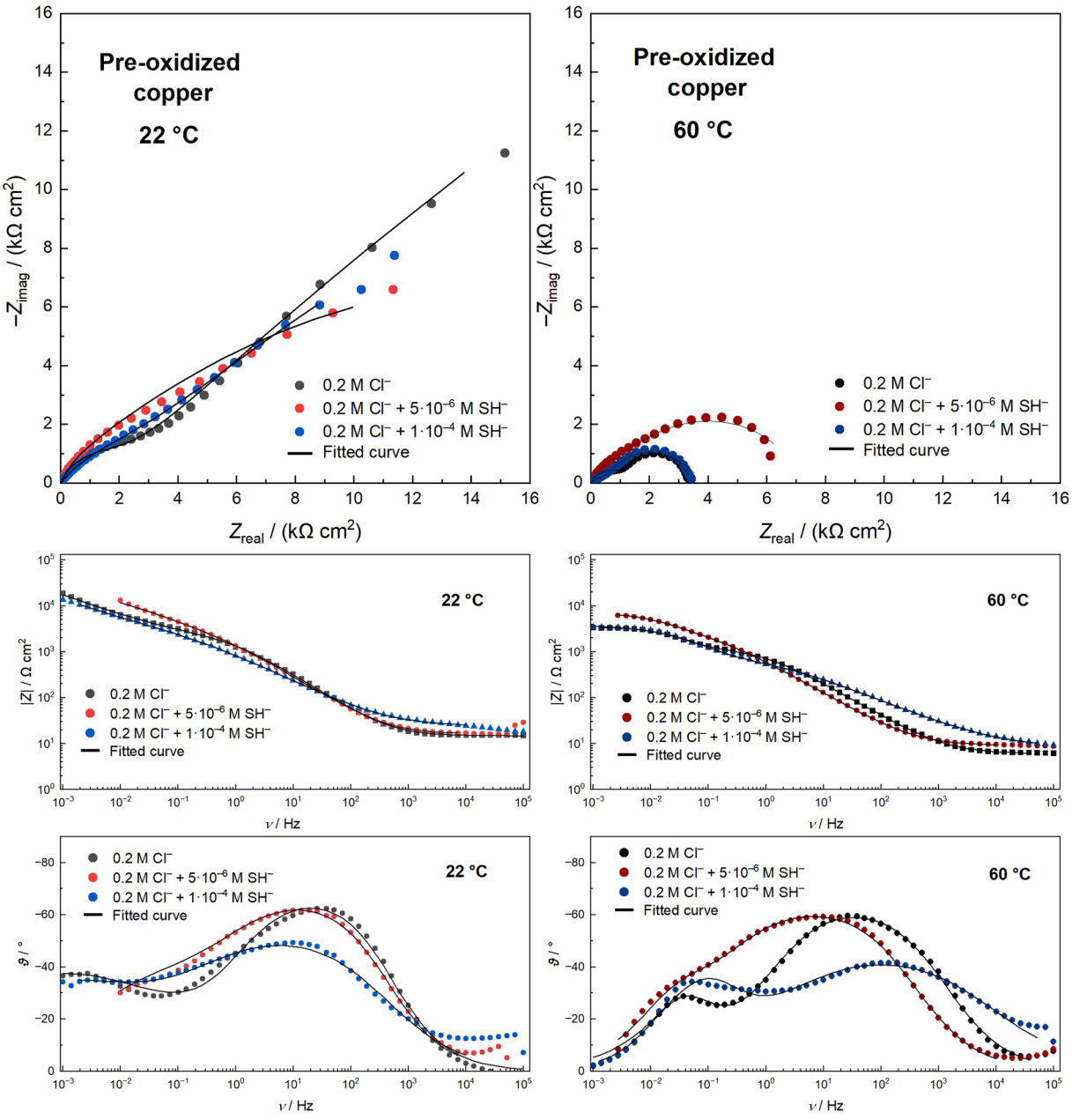

Fig. 4. Nyquist and Bode diagrams of the pre-oxidized copper after 24 h immersion in three different solutions (0.2 M Cl$^-$, 0.2 M Cl$^-$ + 5·10^{-6} M SH$^-$, and 0.2 M Cl$^-$ + 1·10^{-4} M SH$^-$) at 22 °C and 60 °C.

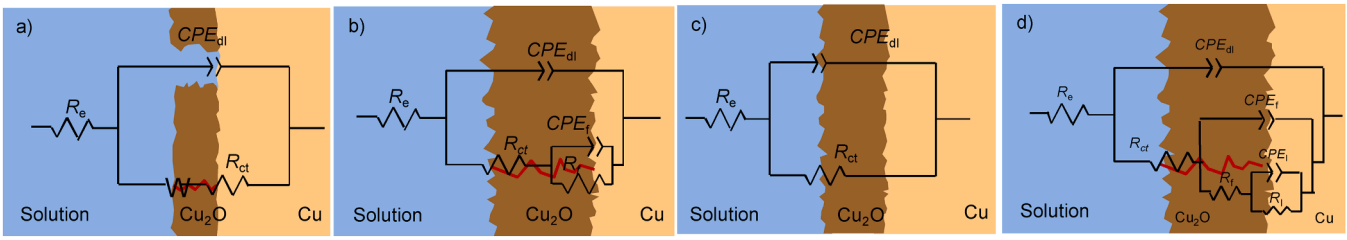

Fig. 5. Equivalent circuits used to fit the EIS spectra obtained on the copper and pre-oxidized copper after 24 h immersion in different solutions at 22 °C and 60 °C. Red line indicates ionic paths through non-protective layer.

Table 1
Results of fitting the EIS spectra obtained with the equivalent electrical circuits shown in Fig. 5 on the copper samples in 0.2 M Cl^-, in 0.2 M Cl^- + 5·10^{-6} M SH^-, and in 0.2 M Cl^- + 1·10^{-4} M SH^-, at 22 °C and at 60 °C.

		R_e Ω cm^2	C_{dl}, μF cm^{-2}	n_{dl}	R_{ct}, Ω cm^2	C_f, μF cm^{-2}	n_f	R_f, Ω cm^2	σ_W, Ωcm^{2}s$^{-1/2}$	C_l, μF cm^{-2}	n_3	R_l, Ω cm^2	*Chi-square*	*Equivalent circuit (in Fig.)*
0.2 M Cl^-	22 °C	17.6	14.3	0.927	70.48	7570	0.831	18,990		652	0.559	5721	0.0000741	5d
	60 °C	9.76	147	0.711	1382	4630	0.939	1799					0.000298	5b
0.2 M Cl^- + 5·10^{-6} M SH^-	22 °C	16.1	126	0.730	5285				1300				0.00031	5a
	60 °C	16.2	206	0.658	6863								0.00116	5c
0.2 M Cl^- + 1·10^{-4} M SH^-	22 °C	9.04	0.043	0.666	376				725				0.000666	5a
	60 °C	2.36	149	0.5	712.4	2290	0.88	2762					0.001093	5b

Table 2
Results of fitting the EIS spectra obtained with the equivalent electrical circuits shown in Fig. 5 on the pre-oxidized copper samples in 0.2 M Cl^-, in 0.2 M Cl^- + 5·10^{-6} M SH^-, and in 0.2 M Cl^- + 1·10^{-4} M SH^-, at 22 °C and at 60 °C.

		R_e Ω cm^2	C_{dl}, μF cm^{-2}	n_{dl}	R_{ct}, Ω cm^2	C_f, μF cm^{-2}	n_f	R_f, Ω cm^2	σ_W, Ωcm^{2}s$^{-1/2}$	*Chi- square*	*Equivalent circuit (in Fig.)*
0.2 M Cl^-	22 °C	14.6	114	0.786	2249				1003	0.0012	5a
	60 °C	5.96	137	0.732	1253	3460	0.889	2157		0.000168	5b
0.2 M Cl^- + 5·10^{-6} M SH^-	22 °C	16.2	141	0.766	1722				1332	0.000223	5a
	60 °C	0.026	437	0.719	3143	1700	0.771	4124		0.000197	5b
0.2 M Cl^- + 1·10^{-4} M SH^-	22 °C	23.5	351	0.607	3525				653	0.000614	5a
	60 °C	8.0	145	0.535	944	1290	0.839	2870		0.000730	5b

two *RCPE* couples (Fig. 5), where R is a resistor and CPE is a constant phase element. A Constant Phase Element (CPE) is used to describe non-ideal capacitive behaviour due to uneven current distribution or surface inhomogeneity providing the exponent n is close to unity. The impedance of the CPE is given by Eq. (7) [68]:

$$Z_{CPE(\omega)} = [C(j\omega)^n]^{-1} \quad (7)$$

R_e represents the electrolyte resistance, $CPE_{dl}R_{ct}$ couple represents the reaction between the metal and the solution at the interface, with CPE_{dl} representing the capacitive properties in the electrochemical double layer and R_{ct} representing the charge transfer resistance.

Q_fR_f represents the properties of and within the oxide layer for surface films grown at 60 °C.

In chloride/sulfide solutions at 22 °C, the Warburg diffusion element was used instead, when n value was 0.5. The Warburg element is given by Barsoukov and Macdonald [50]

$$W_{inf} = \frac{\sigma_W}{\sqrt{\omega}}(1-j) \quad (8)$$

where the Warburg coefficient is related to the surface concentration (c_s) and diffusion coefficient (D) by the equation

$$\sigma_W = \frac{RT}{n^2F^2c_s\sqrt{2D}} \quad (9)$$

where R presents gas constant (8.314 J/mol·K), T (K) temperature, n number of electrons, and F is the Faraday constant (96,544 As/mol).

The CPE_l and R_l couple represents additional loosely bound layer present for Cu in 0.2 M Cl^- solution at room temperature.

Equivalent circuit in Fig. 5a was used to fit impedance spectra for copper and pre-oxidized copper in chloride and chloride/sulfide solutions at 22 °C where diffusion properties were observed in low frequency region, while Fig. 5b represents equivalent circuit used to fit the impedance spectra at 60 °C. Fig. 5c shows the equivalent electrical circuit used to fit the EIS spectra of the copper immersed in the chloride solution with a low sulfide concentration (5·10^{-6} M SH^-) at 60 °C, and Fig. 5d presents equivalent electrical circuit for fitting the EIS spectra for Cu in 0.2 M Cl^- at 22 °C.

The fitted parameter values are summarized in Tables 1 and 2. Z_{CPE} was converted to an effective capacitance using the relationship derived by Brug [69].

The capacitance C_{dl} values are in the range 100–400 μF/cm^2 in solutions with sulfide ions, while the C_{dl} value for Cu and pre-oxidized copper in 0.2 M Cl^- is smaller at 14 and 114 μF/cm^2, respectively.

Such values may reflect surface roughening. Generally, higher values are observed at higher temperatures (see Tables 1 and 2).

For the experiments at room temperature (22 °C), the equivalent circuit in Fig. 5a is attributed to the diffusion of O_2 through the oxide layer. When observing the Warburg coefficient (σ_W), it can be seen that very similar values were observed; between 1.00 and 1.33 kΩ cm^2 $s^{-1/2}$ for copper and pre-oxidized copper in 0.2 M Cl^- with $5{\cdot}10^{-6}$ M SH^-, and 0.6–0.7 kΩ cm^2 $s^{-1/2}$ for copper and pre-oxidized copper in higher sulfide concentration (0.2 M Cl^- with $1{\cdot}10^{-4}$ M SH^-) at 22 °C. Similar values show similar surface concentration, c_s of O_2 and similar effective diffusion coefficient (D) within developed porous layer (see Tables 1 and 2).

At elevated temperatures (60 °C) no diffusion tail was observed in the Nyquist plots, indicating that the diffusion-controlled process is no longer dominant under these conditions. At low frequency region, the value of R_f can be observed in chloride-sulfide systems at 60 °C, with values between 1800 and 4000 Ω cm^2. The difference can be noticed between copper and pre-oxidized copper, with slightly higher values for pre-oxidized copper (see Tables 1 and 2).

With presented EIS measurements after 24 h, variations in the measured impedances may no longer occur when the effect of the sulfide has taken place and the sulfide has been consumed. Possibly, this competes with the reaction of SH^- at the surface or its oxidation in the solution to either S_8 or sulfates [70,71]. How these surface films changed with time was not recorded, but it has been shown previously in a shorter experiment that the impedance response for Cu in 3 % NaCl and $3{\cdot}10^{-5}$ mol/L S^{2-} increases with the immersion time [3].

It this study we have focused on particular time after 24 h exposure to chloride and chloride/sulfide solutions with comparison to spectroscopic data, presented below.

3.3. *Exposure of the pre-oxidized copper samples to chloride solutions with different sulfide concentration at room (22 °C) and elevated (60 °C) temperatures*

Copper samples with preformed Cu_2O were immersed in chloride solutions containing different sulfide concentrations for 24 h under aerated conditions. The sulfide concentrations were $5{\cdot}10^{-6}$ M SH^- and $1{\cdot}10^{-4}$ M SH^-, respectively. The samples were exposed to conditions at room temperature (22 °C) and an elevated temperature (60 °C). Before immersion, the copper samples were oxidized to form Cu_2O on the surface so as to mimic the oxidation of copper in an unpolluted humid atmosphere. Details of the pre-oxidation steps are given in the Materials and methods section.

Fig. 6 shows the pre-oxidized copper samples after 24 h of immersion in the chloride solutions and in the solutions with different sulfide concentrations at 22 °C and 60 °C. Differences between the surface color of the various samples and at different temperatures can be observed.

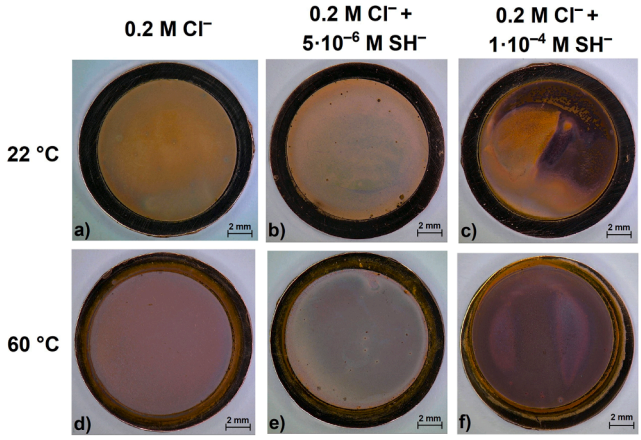

Fig. 6. Surfaces of the pre-oxidized copper samples after 24 h immersion in the chloride solutions with different sulfide concentrations at 22 °C and 60 °C: a, d) 0.2 M Cl^-, b, e) 0.2 M Cl^- $5{\cdot}10^{-6}$ M SH^-, and c, f) 0.2 M Cl^- + $1{\cdot}10^{-4}$ M SH^-.

At room temperature, the surface of the pre-oxidized sample in the 0.2 M Cl^- solution is orange-brown in color. When the sample was placed in a solution with a low sulfide concentration ($5{\cdot}10^{-6}$ M SH^-) the surface darkened, while in the solution with a high sulfide concentration ($1{\cdot}10^{-4}$ M SH^-) approximately 50 % of the surface became black in color.

At 60 °C it can be observed that the surfaces of the samples are darker in color. The surface of the sample that was immersed in the chloride solution was rather dark and reddish-purple in color. When the sample was immersed in the solution with a low sulfide concentration at 60 °C, the surface became slightly darker and browner. At the highest sulfide concentration, the entire surface of the pre-oxidized sample became dark purple to almost black in color.

The changed colors of the surface films clearly show the changes in the composition and texture of the surface, and, indirectly, differences in the thickness of the films.

SEM images of the surface morphology of the corrosion films on the pre-oxidized copper after immersion in a chloride solution without the addition of sulfide are shown in Fig. 7. At room temperature, the corrosion film followed the grinding grooves still visible on the surface, as shown in Fig. 7a. The corrosion products, in the form of cubic crystals, varied in size and shape and were not evenly distributed across the surface. Some pits were also observed on the surface. The cubic crystals ranged in size from 0.15 μm to 0.7 μm. The chemical composition of the cubic crystals was determined by EDS analysis. It was found that the larger crystals consisted of 10.6 wt. % O and 89.4 wt. % Cu (area 1), while the remaining surface area, with smaller corrosion products, consisted of 6 wt. % O and 94 wt. % Cu (area 2). Similar behavior with respect to the formation of corrosion products was observed in a study by Ratia-Hanby [50], where the formation of a film in simulated groundwater, either without the addition of sulfide or in a solution with a low sulfide concentration, also followed the grinding grooves.

At elevated temperature, the corrosion products were larger in size and more homogeneously distributed across the surface (Fig. 7b). The size of the cubic crystals ranged between 0.2 μm and 2.4 μm. Larger cubic crystals were found to consist of 13.8 wt. % O and 86.3 wt. % Cu (area 3). The area with smaller corrosion particles, area 4, consisted of 10.6 wt. % O and 89.4 wt. % Cu. Kosec et al. [15] found that the corrosion products found on a Cu-sheet after immersion in a 0.1 M NaCl solution for 30 days primarily consisted of Cu_2O and took the form of irregular cubic crystals.

At room temperature, the corrosion products accumulated following the grinding grooves in the solution with a low sulfide concentration ($5{\cdot}10^{-6}$ M SH^-) (Fig. 8a). The visibility of the grinding grooves indicated the presence of a relatively thin film of corrosion products. The corrosion products were in the form of cubic crystals and varied in size from 0.15 μm to 1.1 μm. Compared to the sample that was immersed in only the chloride solution, the cubic crystals were larger and the surface on this sample was free of pits. EDX maps showed that the surface in area 1 consisted of 10.9 wt. % O and 89.1 wt. % Cu. Smaller corrosion products in area 2 resembled the chemical composition of larger cubic crystals.

Two different morphologies of corrosion products were observed on the pre-oxidized copper sample immersed in the chloride solution with a low sulfide concentration at 60 °C, as shown in Fig. 8b Larger cubic crystals, between 0.45 μm and 3 μm in size, uniformly covered the surface, with small corrosion products in the form of needles formed on top. Thinner and thicker needle-like corrosion products formed as crystal structures and covered several cubic-shaped corrosion products. The length of the thicker needles was observed to be >8 μm. EDX maps showed that the needle-like corrosion products contained more sulfur. This was also observed in the EDS analysis of the acicular corrosion products, which proved the presence of S. In area 3 (Fig. 8b), the analysis showed the presence of 2.8 wt. % S, 13.1 wt. % O, and 84.1 wt. % Cu. The remaining area was similar but contained less sulfur. The EDS

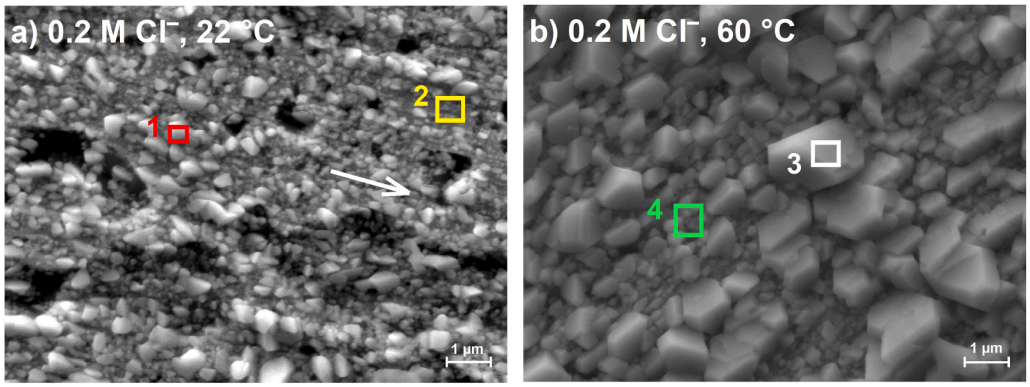

Fig. 7. SEM images of the pre-oxidized copper samples immersed in the 0.2 M Cl^- solution at 22 °C (a) and 60 °C (b) for 24 h.

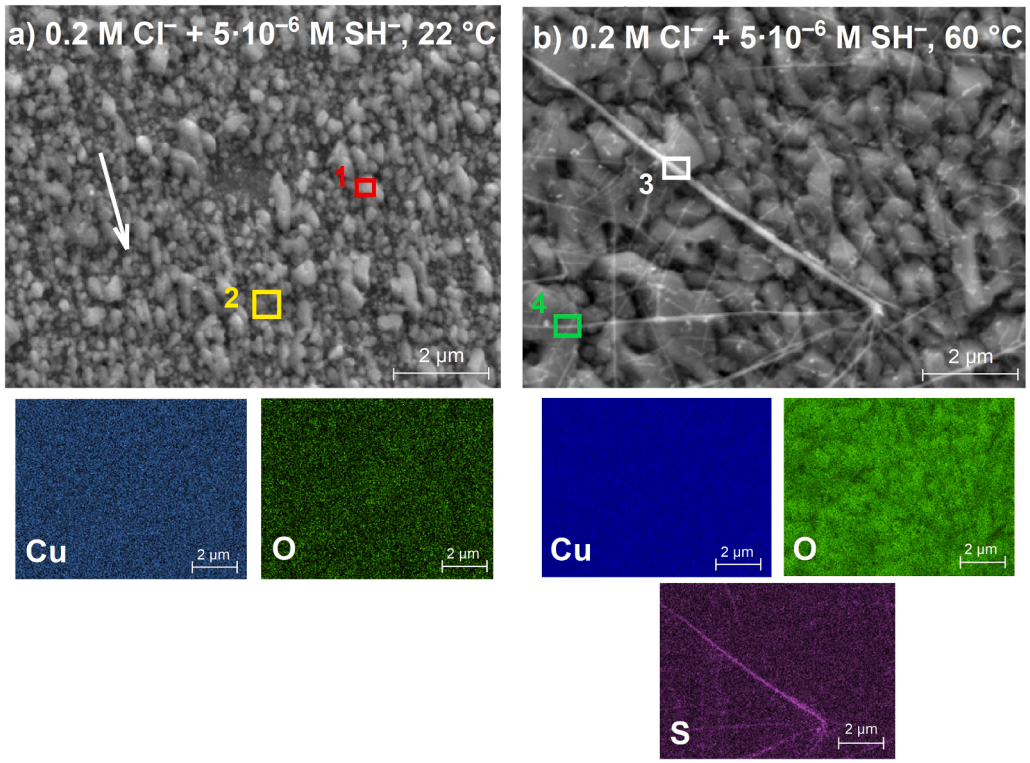

Fig. 8. SEM images of the pre-oxidized copper samples exposed to a 0.2 M Cl^- solution with a low sulfide concentration (containing $5{\cdot}10^{-6}$ M SH^-) at 22 °C (a) and 60 °C (b) for 24 h.

analysis of area 4 in Fig. 8b showed that the corrosion products contained 0.6 wt. % S, 13.7 wt. % O, and 85.7 wt. % Cu.

The morphology of the corrosion products in the solution with the highest sulfide concentration ($1{\cdot}10^{-4}$ M SH^-) differs from that observed on the pre-oxidized copper samples immersed in solutions with a low concentration or in those containing no sulfide. At room temperature, various agglomerates of sulfur-containing corrosion products are observed, as seen in Fig. 9a (shown in the EDX maps). Smith et al. [47] observed sponge-like deposits after 24 h of immersion in an anoxic solution containing 10^{-3} mol/L sulfide, indicating the ongoing accumulation of a thick outer layer on the deposit. The agglomerates of corrosion products varied in size from 2.3 µm to 7 µm and were in the shape of different dendritic and columnar deposits. The EDS analysis of the larger agglomerates (area 1) showed consistently higher concentrations of S (4.4 wt. %), as shown in Fig. 9a. The EDS analysis also showed the presence of O (11.9 wt. %) and Cu (83.7 wt. %). The rest of the small corrosion products on the surface (area 2) exhibited lower concentrations of S (2.4 wt. %) and O (8 wt. %) and higher concentrations of Cu.

At 60 °C, corrosion products of different morphologies were present, as seen in Fig. 9b Large and well-defined cubic crystals with smooth surfaces and fine agglomerates could be observed. The size of the cubic corrosion products on the surface was between 1.5 µm and 9.3 µm. A different film morphology was formed on top of the cubic crystals. The size of the agglomerates was between 0.5 µm and 1 µm and they were distributed like moss, covering the cubic crystals. The EDX maps showed that the film over the cubic crystals contained more sulfur, which was also confirmed by the EDS analysis. The cubic corrosion products shown in area 4 consist of 15.4 wt. % O, 84.2 wt. % Cu, and only 0.4 wt. % S. The agglomerate film on the cubic crystals contained more sulfur (5.2 wt. %) and less oxygen (10.6 wt. %).

The corrosion products formed on the pre-oxidized copper surface were identified by Raman spectroscopy. Fig. 10 depicts the spectra obtained on the pre-oxidized copper samples after 24 h immersion in

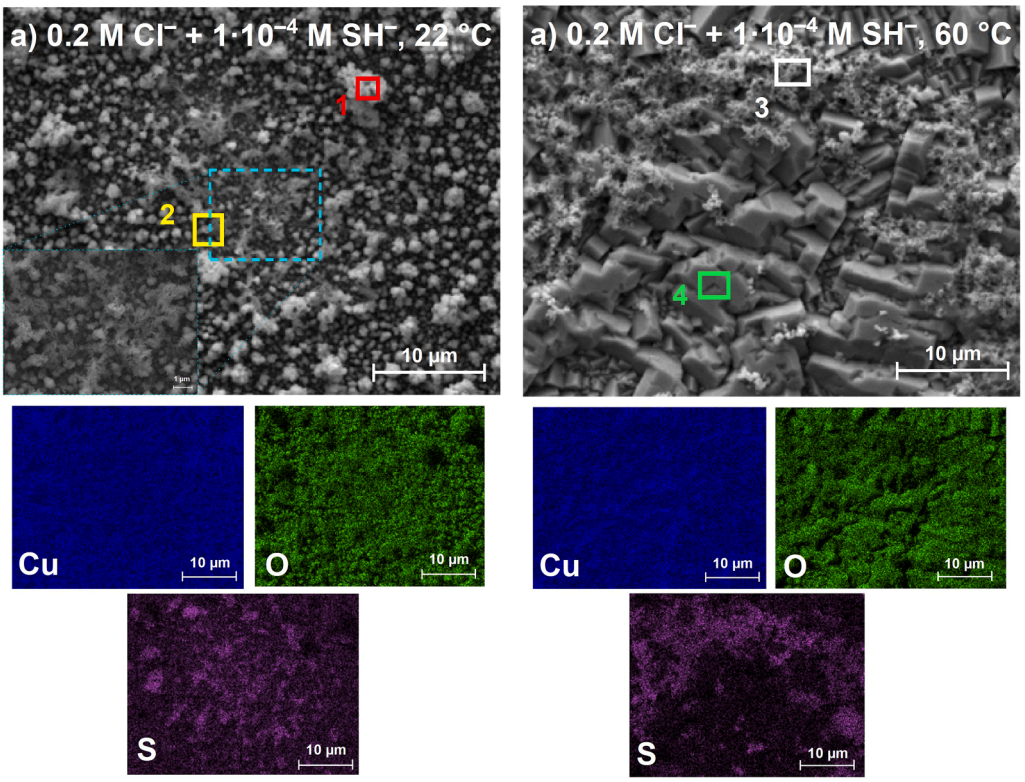

Fig. 9. SEM images of the pre-oxidized copper samples exposed to a 0.2 M Cl^- solution with a high sulfide concentration ($1{\cdot}10^{-4}$ M SH^-) at 22 °C (a) and 60 °C (b) for 24 h.

various chloride solutions with different sulfide concentrations at room and elevated temperatures. The Raman spectra of the pre-oxidized copper immersed in a chloride solution for 24 h demonstrate the presence of Cu_2O, with bands at 149 cm^{-1}, 221 cm^{-1}, 401 cm^{-1}, 528 cm^{-1}, and 632 cm^{-1} (Fig. 10a) [72–74]. The Raman spectra also indicate the presence of Cu_2O at a higher temperature, with bands positioned at the same wavelengths, as shown in Fig. 10b

When a small quantity of sulfide ($5{\cdot}10^{-6}$ M SH^-) was added to the chloride solution at room temperature, the Raman spectra showed the presence of Cu_2O, but no band indicative of Cu_2S was observed. The bands for Cu_2O are observed at 146 cm^{-1}, 218 cm^{-1}, 528 cm^{-1}, and 627 cm^{-1} (Fig. 10c). At elevated temperature, however, a small additional band appeared at 289 cm^{-1}, which was attributed to Cu_2S (Fig. 10d) [75, 76]. The presence of sulfide was also indicated by EDS analysis, while Raman spectroscopy confirmed its presence on the surface.

When a greater amount of sulfide ions ($1{\cdot}10^{-4}$ M SH^-) was added to the chloride solution at room temperature, darker, almost black corrosion products appeared. The Raman spectra of the black corrosion products (area 3 on Fig. 10e) showed only one band for Cu_2S, at 282 cm^{-1}, and none for Cu_2O. In areas 1 and 2, the bands for Cu_2O were observed at 146 cm^{-1}, 217 cm^{-1}, and 631 cm^{-1}, and a band for Cu_2S was also observed at 285 cm^{-1}. At 60 °C, the Raman spectra indicated the presence of Cu_2O, and the band for Cu_2S was also observed at 282 cm^{-1} (Fig. 10f).

The thickness of the corrosion film was analyzed by FIB-SEM, as shown in Fig. 11. Fig. 11a shows a pre-oxidized copper sample immersed in the chloride solution for 24 h at room temperature. The analysis revealed the thickness of the corrosion film to be 74 to 120 nm. At 60 °C, the thickness of the corrosion layer ranged from 270 nm (small corrosion products) to 560 nm (larger cubic crystals of Cu_2O, as indicated by the Raman spectra), as shown in Fig. 11b

When the pre-oxidized copper sample was immersed in a solution with a low sulfide concentration ($5{\cdot}10^{-6}$ M SH^-), the corrosion layer was coated with Pt to facilitate observation of the cross section (Fig. 11c). The analysis enabled the observation of a few individual gaps between the copper and the corrosion layer. The size of the gaps was between 80 and 250 nm. At 22 °C, the corrosion layer was between 89 and 380 nm in size. At an elevated temperature, the thickness of the corrosion layer ranged from 169 nm to 540 nm (Fig. 11d). The thickness of the small corrosion products, in the form of needle-shaped structures, was up to 160 nm.

The thickness of the corrosion film formed on the pre-oxidized copper sample immersed in the solution with the highest sulfide concentration ($1{\cdot}10^{-4}$ M SH^-) was 1.78 to 6.68 µm, as shown in Fig. 11e. Since it was difficult to create a cross section of the thick corrosion film, which contained sulfur, and to avoid decomposition under electrons and Ga^+ ions, the film was coated with Pt, similar to as done in a previous study [79]. As shown in Fig. 11e, the sulfur-containing corrosion deposits grew in the form of a columnar film in the vertical direction. The smaller corrosion layer was 120 to 520 nm thick, and the columnar film, which can be seen to be porous, grew up to 6.68 µm. At an elevated temperature, the thickness of the corrosion layer attributed to Cu_2O was 1.92 µm (Fig. 11f). The corrosion products formed on the cubic crystals, which, according to the EDS analysis, contained more sulfur, were about 335 nm thick. In addition, a far more significant gap can be observed between the Cu base metal and the corrosion layer. Martino et al. [51] also observed a detachment of the base layer from the Cu substrate, which they attributed to the removal of the sample from the electrochemical cell and the drying process. A large void was also observed between the porous base layer and the outer layer, but they were uncertain as to whether the void formed due to stresses created at the corrosion interface as the thick, porous layer grew.

3.4. Cathodic stripping voltammetry of the pre-oxidized copper samples after 24 h immersion in various chloride solutions with different sulfide concentrations

Cathodic stripping voltammetry (CSV) was performed to obtain

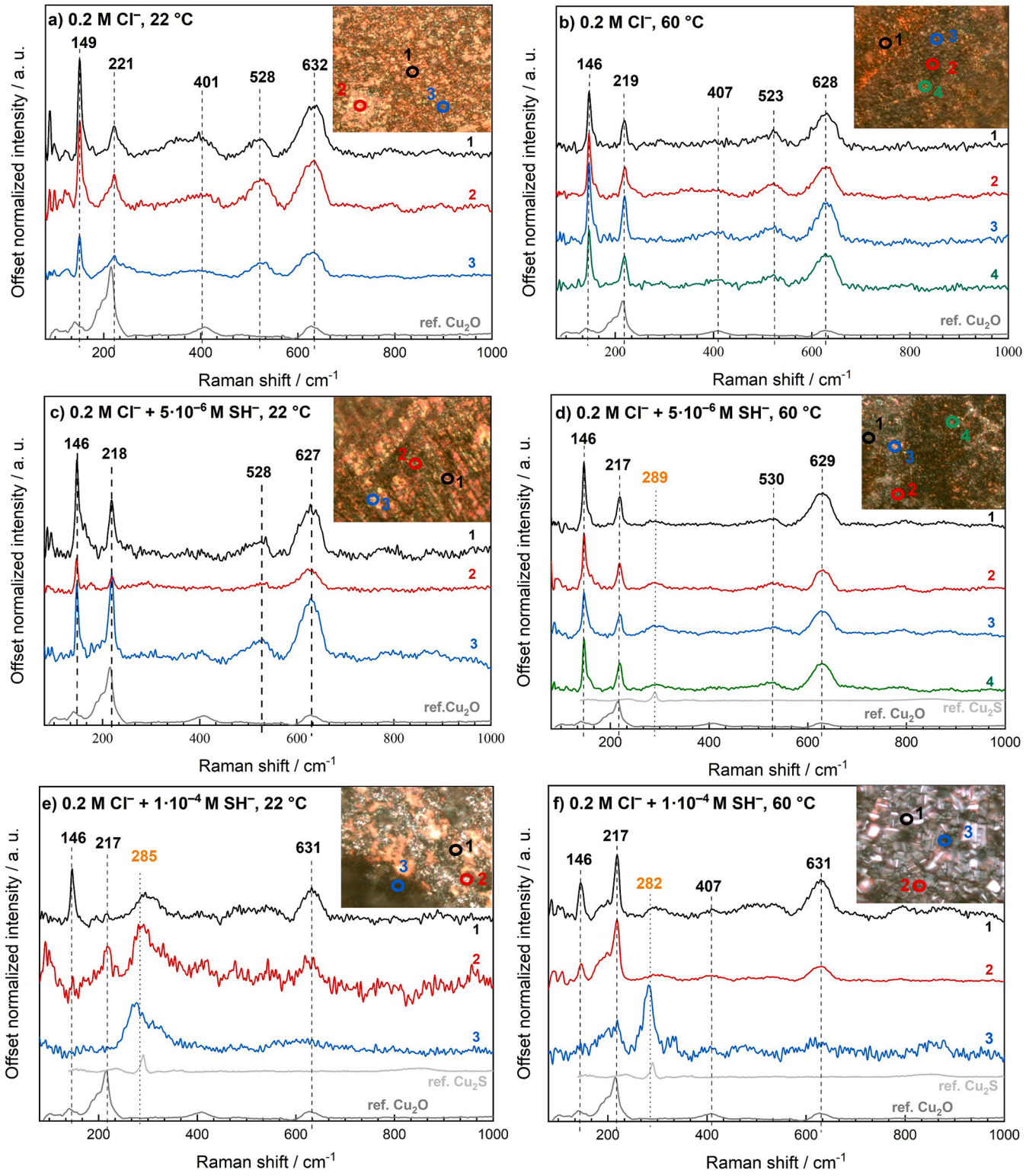

Fig. 10. Raman spectra of the corrosion products formed on the pre-oxidized copper samples after 24 h immersion in solutions containing (a, b) 0.2 M Cl^-, (c, d) 0.2 M Cl^- + 5·10^{-6} M SH^-, and (e, f) 0.2 M Cl^- + 1·10^{-4} M SH^- at 22 °C (a, c, e) and 60 °C (b, d, f), alongside ref. Cu_2O, cuprite [77] and ref. Cu_2S, chalcocite as analyzed in [77] and as posted in [78].

information about the reduction processes on the pre-oxidized copper samples after immersion in various chloride solutions with different sulfide concentrations at room (22 °C) and elevated (60 °C) temperatures. Fig. 12 shows the CSV curves of the various pre-oxidized copper samples immersed in a chloride solution, in a chloride solution with the addition of 5·10^{-6} M SH^-, and in a chloride solution with 1·10^{-4} M SH^- added. Cathodic stripping voltammetry was performed from 0 V to –1.5 V, and the thickness of the film was obtained from the charge densities, calculated using Eq. (1). Details for obtaining the thickness of the film are given in the Materials and methods section.

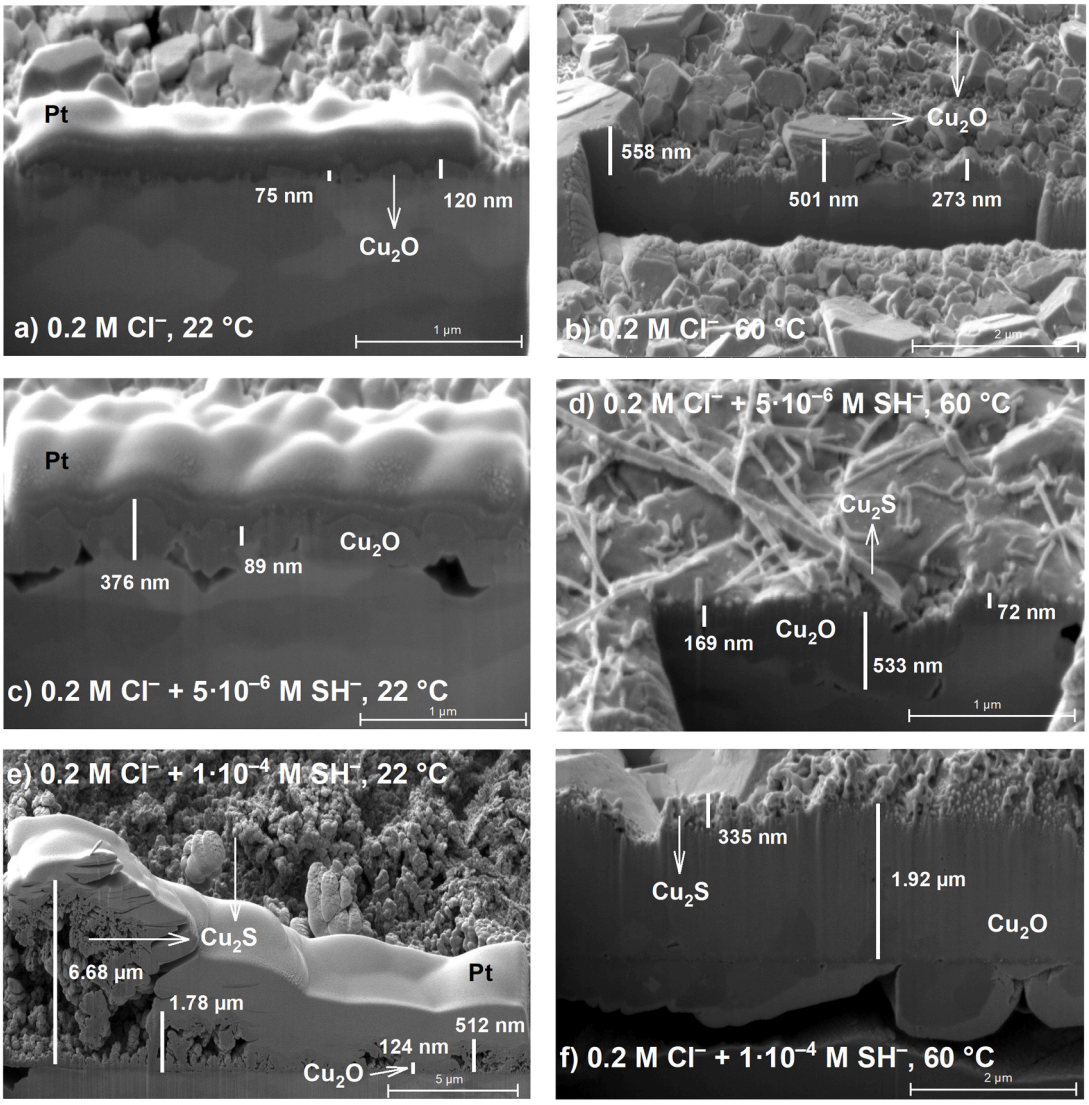

Fig. 11. FIB-SEM images of the pre-oxidized copper sample after 24 h immersion in the various solutions ((a, b) 0.2 M Cl^-, (c, d) 0.2 M Cl^- + $5{\cdot}10^{-6}$ M SH^-, and (e, f) 0.2 M Cl^- + $1{\cdot}10^{-4}$ M SH^-) at 22 °C and 60 °C.

Fig. 12a shows the pre-oxidized copper samples that were exposed to a chloride solution at 22 °C and 60 °C. At both temperatures, one cathodic peak was observed, which can be attributed to the reduction of Cu_2O. This can be inferred from the surface characterization shown both in this paper and from the literature [54]. At room temperature, the peak appeared at a potential of $E = –0.81$ V, while at an elevated temperature, the peak shifted to more negative values, at a potential of $E = –0.95$ V. The thickness of the corrosion film was calculated from the charge obtained under the curve. The thickness of the Cu_2O film was 78 nm at room temperature and 501 nm at an elevated temperature. Very good agreement was shown between the thickness estimated by FIB-SEM observation and that calculated from the charge densities.

At room temperature, when a small amount of sulfide ($5{\cdot}10^{-6}$ M SH^-) was added to the 0.2 M chloride solution, a peak at $E = –0.91$ V was observed on the CSV, as shown in Fig. 12b The peak was attributed to the reduction of Cu_2O and the thickness was calculated to be 150 nm. Another reduction peak could be observed at the elevated temperature. The first reduction peak at $E = –0.99$ V, attributed to Cu_2O, shifted to more negative values. The additional reduction shoulder was observed at more negative potentials ($E = –1.12$ V), which can be attributed to the reduction of Cu_2S. The thickness of the Cu_2O layer was calculated to be 279 nm and the thickness of the Cu_2S 1.5 nm. Kosec et al. [80] observed a large peak between –1.0 V and –1.1 V after 24 h of CSV for copper exposed to a solution of 0.1 M Cl^- + $5{\cdot}10^{-6}$ M SH^-, confirming that the initially formed Cu_2S/Cu_2O layer was not passive and allowed greater expansion of the outer deposited layer. In the presence of sulfide ions—which strongly promote the growth of the outer deposited layer—the thicknesses derived from CSV curves serve only as rough estimates. Due to poor contact between the corrosion film and the Cu substrate, the reduction process may be incomplete, leading to an underestimation of the thickness of Cu_2S layer.

In the chloride solution with a high sulfide concentration (containing $1{\cdot}10^{-4}$ M SH^-), two reduction peaks were observed in the CSV curve at room temperature (Fig. 12c). The first reduction peak appeared at a potential of $E = –0.90$ V, which was, again, attributed to the reduction of Cu_2O. The second peak was attributed to the reduction of Cu_2S (confirmed also by Raman spectroscopy), which appeared at a potential of $E = –1.08$ V. The thickness of the Cu_2O film calculated from the charge densities was 269 nm and the thickness of the Cu_2S film was 15 nm. At higher temperatures, a cathodic peak with a shoulder at a more negative potential can be observed. The first reduction peak, at a potential of $E = –1.18$ V, was attributed to the reduction of Cu_2O. The thickness calculated from the charge densities was 549 nm. The additional shoulder was observed at a more negative potential of $E = –1.31$ V

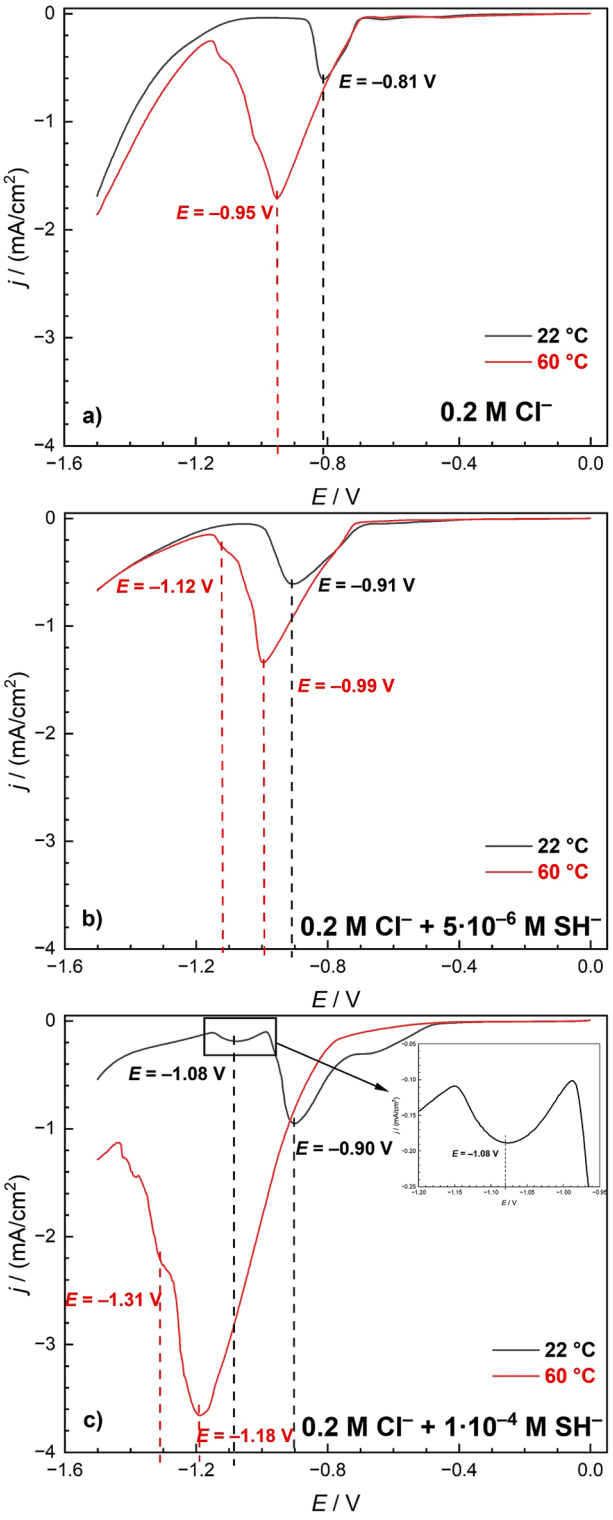

Fig. 12. CSV of the pre-oxidized copper immersed in different solutions for 24 h at 22 °C and 60 °C: a) 0.2 M Cl^-, b) 0.2 M Cl^- + $5{\cdot}10^{-6}$ M SH^-, and c) 0.2 M Cl^- + $1{\cdot}10^{-4}$ M SH^-. CSV was performed in a borate buffer at a scan rate of 1 mV/s.

and is attributed to the reduction of Cu_2S. It could be seen that more complex reduction reactions were taking place. The thickness of the Cu_2S layer was calculated to be 21 nm.

CSV enabled the identification of reduction species; however, particularly in cases where a thick outer deposit was present—as confirmed by FIB-SEM analysis—the charge-based estimations from CSV diagrams should be considered comparative rather than absolute.

3.5. Model of corroding system

The corrosion rate of copper is governed primarily by the ionic-transport properties of its corrosion-product film. Using FIB-SEM, we characterized the morphology and thickness of films on Cu and pre-oxidized Cu after exposure to (i) a chloride solution and (ii) the same chloride solution contaminated with sulfide (SH^-) at two temperatures (22 °C and 60 °C).

Although the standard Gibbs free energies of formation suggest that Cu_2O (ΔGf° = –141 kJ mol^{-1}) should be more stable than Cu_2S (ΔGf° = –98 kJ mol^{-1}) [81], thermodynamics alone does not explain the loss of protectiveness observed when SH^- is present. FIB-SEM cross-sections showed that sulfide accelerated the transition from a compact, low-permeability Cu_2O layer to a heterogeneous, defect-rich film containing Cu_2S, through which ionic transport is orders of magnitude faster.

This behavior is consistent with Payer's four-stage model [82]. In the first and second stage, a thin, compact Cu_2O layer forms in air or solution. Its low ionic conductivity suppresses corrosion by blocking ion transport. In the third stage, the film loses protectiveness. Sulfide ions (SH^-) promote Cu_2S formation and increase structural defects, resulting in a heterogeneous layer with higher ionic transport. This shift enables corrosion to proceed. In the fourth stage, a porous outer layer forms over the inner, now non-protective layer. Though thicker (in the μm range), this layer allows ionic movement and water ingress, sustaining active corrosion beneath.

The schematic representation in Fig. 13 shows the electrochemical and spectroscopic findings for the pre-oxidized Cu immersed in sulfide-polluted saline solutions in oxic conditions. The protective properties of the Cu_2O layer are lost in chloride solutions and this becomes even more evident when low quantities of sulfide ions are added. This can be seen in the porous structure with a surface opening at the Cu/Cu_2O interface and in the increased ionic conductivity observed with the thickening of the film. At higher sulfide concentrations, a porous and thick Cu_2O/Cu_2S film was formed, and tarnishing was also observed.

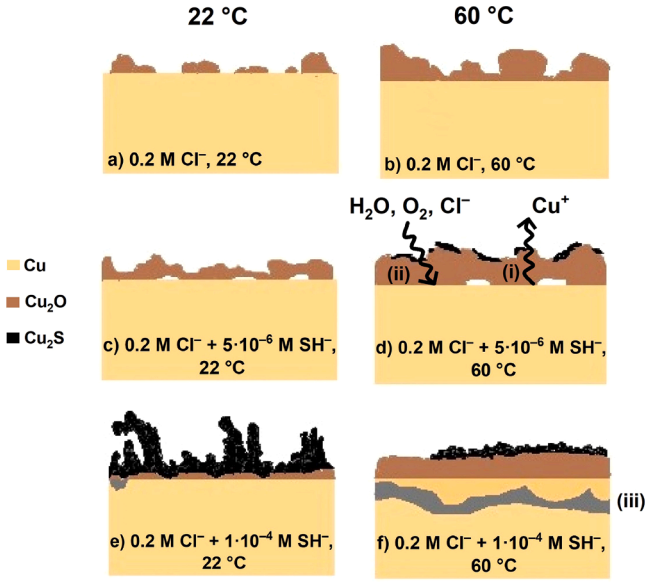

Fig. 13. Schematic representation of the pre-oxidized copper in chloride solutions with different sulfide concentrations at 22 °C and at 60 °C. Processes taking place at Cu/inner interface: (i) oxidation of Cu: Cu→ Cu^+ + 1 e^-, (ii) reduction of oxidizing species (22 °C) O_2 + 2 H_2O + 4 e^-→ 4 OH^-, (iii) reduction reaction taking place at 60 °C: 2 H^+ + 2 e^- → H_2.

3.5.1. Effect of pre-oxidizing of copper

Electrochemical oxidation at –0.19 V in borate buffer resulted in formation of a 15 nm thick Cu_2O, which is protective due to its p-type conducting nature [83]. However, FIB-SEM analysis of cross sections revealed notable changes after immersion in 0.2 M Cl^- solution. After 24 h, the surface film on the pre-oxidized Cu became porous and significantly thicker reaching 75–120 nm. This increase in thickness coincides with a loss of the protective properties. The degradation is attributed to changes in the semiconductor character of the oxide: the initially uniform p-type Cu_2O layer evolved into a mixed oxide with spatially separated p-type and n-type regions. In particular, the formation of n-type Cu_2O at the metal/oxide interface facilitates ionic transport, compromising the barrier properties of the film [64,83].

With the pre-oxidized copper, the initial corrosion potential at 22 °C was more positive than that observed for copper. That was observed for all the solutions, 0.2 M Cl^- and 0.2 M Cl^- with the addition of $5{\cdot}10^{-6}$ M SH^- and $1{\cdot}10^{-4}$ M SH^-. The decreasing potential indicated the destabilizing effect of the oxide film, which transforms in a saline solution. After 24 h of immersion, the corrosion potential of the pre-oxidized copper was similar to that of copper in a chloride solution (–0.19 V), which stabilized already after 8 h of immersion.

Under deaerated conditions, corrosion proceeds via a different mechanism, with sulfide ions acting as the anodic reactant and water reduction driving cathodic process, leading to the conversion of Cu_2O to Cu_2S [45,47,51,84,85]. The pre-formed Cu_2O layer (oxidation at –0.3 V) delayed the three-stage transition from –0.41 V to –0.9 V, during which Cu_2O gradually transformed into Cu_2S [45,47].

The impedance results (Tables 1 and 2) and R_{ct} values further confirm that the film that formed on pre-oxidized copper showed destabilizing properties after 24 h, with similar values of R_{ct} of 3–5 kΩ cm^2 (Tables 1 and 2). However, from FIB-SEM results, we could observe that film thickness increased after 24 h exposure, from 15 nm to 75–120 nm in 0.2 M Cl^-, to 89–376 nm in 0.2 M Cl^- + $5{\cdot}10^{-6}$ M SH^- and even more (124–512 nm (Cu_2O) and 1.78–6.68 μm (Cu_2S)) in 0.2 M Cl^- + $1{\cdot}10^{-4}$ M SH^-. The measured thickness of the FIB-SEM cross section corresponded to the thickness calculated from the estimated charge of the peaks in the cathodic stripping voltammograms for Cu_2O only, as is evident from the Table 3.

In general, the pre-oxidized Cu did not show better protection than Cu under the same conditions.

3.5.2. The effect of temperature

At 60 °C, no significant difference in behavior was observed when measuring the corrosion potential of Cu and pre-oxidized Cu. The evolution of the corrosion potential was quite similar, with the potential increasing slightly in the chloride solutions with a low sulfide concentration (with this difference more pronounced in the pre-oxidized copper).

The surface films were significantly thicker at 60 °C (Table 3, Fig. 11) with the surface deposition of Cu_2S more pronounced. At 60 °C, the Cu_2S was deposited on the surface of the Cu_2O in the form of elongated, needle-like crystals at lower sulfide concentration (Fig. 11d) and fine agglomerates at high sulfide concentration (Fig. 11f). The capacitance values for charge transfer reactions and oxide films in the solution with a low sulfide concentration were even higher at 60 °C (Table 2).

It was observed that at elevated temperatures in sulfide-containing solutions, the cathodic reaction typically involves proton reduction from bisulfide dissociation and SH^- oxidation in O_2 containing solutions [80,86]. This promotes hydrogen evolution at the Cu/film interface (Equation 10):

$$2H^+ + 2e^- \rightarrow H_2 \quad (10)$$

The formation of hydrogen gas may create localized pressure beneath the inner layer, leading to mechanical disruption, such as crack formation and delamination, as observed in Figs. 11f and 13f.

Table 3
Comparison of FIB-SEM cross-sectional analysis of corrosion products after 24 h immersion and thickness evaluated from CSV curves.

	Solution	T	FIB-SEM	CSV	correlation
Cu_2O-15 nm	0.2 M Cl^-	22 °C	75–120 nm	78 nm	good
	0.2 M Cl^- + $5{\cdot}10^{-6}$ M SH^-	22 °C	89–376 nm	150 nm (Cu_2O)	good
	0.2 M Cl^- + $1{\cdot}10^{-4}$ M SH^-	22 °C	124–512 nm (Cu_2O) 1.78–6.68 μm (Cu_2S)	269 nm (Cu_2O) 15 nm (Cu_2S)	good for Cu_2O poor for Cu_2S
	0.2 M Cl^-	60 °C	273–558 nm	501 nm	good
	0.2 M Cl^- + $5{\cdot}10^{-6}$ M SH^-	60 °C	169–533 nm (Cu_2O) 72 nm (Cu_2S)	279 nm (Cu_2O) 1.2 nm (Cu_2S)	good for Cu_2O poor for Cu_2S
	0.2 M Cl^- + $1{\cdot}10^{-4}$ M SH^-	60 °C	1.92 μm (Cu_2O) 335 nm (Cu_2S)	549 nm (Cu_2O) 21 nm (Cu_2S)	good for Cu_2O poor for Cu_2S

3.5.3. The effect of sulfide ions

When sulfides were added to chloride solution, a thick tarnish film and the increased thicknesses of surface deposits analyzed by FIB-SEM microscopy was observed.

The formation of a thick tarnish layer (Fig. 6b–F) marks the transition from a protective oxide to a non-protective mixed oxide/sulfide film [82]. This loss of protection is linked to changes in semiconducting behavior, where sulfide incorporation leads to spatial separation of n-type and p-type regions in Cu_2O. Notably, n-type Cu_2O at the metal/oxide interface facilitates ionic transport, compromising the barrier properties [64,82,87]. This was observed indirectly by examining the cross sections and the large surface population of fine structure across the entire surface and the identification of a Raman band at 285 cm^{-1}, confirming the presence of Cu_2S (Fig. 10f).

The Cu_2O film formed in the solution containing $5{\cdot}10^{-6}$ M SH^- was thicker (up to 376 nm) than that in chloride solution and exhibited large, porous, surface cracks at the Cu/Cu_2O interface. While sulfide was not incorporated, it reduced the film density, leading to high capacitance values (C_{dl}) indicative of elevated ionic conductivity. Prior studies in anaerobic SH^- conditions also showed that Cu_2S formed at low SH^- concentrations is porous [88].

In the chloride solution with a high sulfide concentration ($1{\cdot}10^{-4}$ M SH^-) the FIB-SEM cross sections showed large agglomerates of sulfide structures formed on the surface. The Cu/Cu_2O interlayer was also affected, as large openings were observed (Fig. 11e,F). The film was up to several μm thick, which was also indicated by the high capacitance values shown by the impedance results (Table 2).

The effects of the low and high sulfide concentrations on corrosion potential were negligible after 24 h; only for the pre-oxidized copper in a solution with a low sulfide concentration was the potential slightly more positive (–0.15 V). The impedance results for the Cu and pre-oxidized Cu exposed to chloride solutions with a high sulfide concentration ($1{\cdot}10^{-4}$ M SH^-) show that the sulfide has no significant effect on the properties of the surface oxide film compared to the chloride solution alone. The destabilizing effect of surface film is reflected in lower R_{ct} values for high sulfide concentrations, and even lower for measurements at 60 °C (Tables 1 and 2).

Previous publications have shown that the susceptibility of copper-nickel alloys to corrosion in sulfide-polluted seawater (whether aerated or deaerated), as measured by the polarization resistance, is lower than that in unpolluted seawater under the same conditions [89]. While sulfide ions promote the corrosion of copper [3,20,90], some studies report more complex behavior. For instance, Cu_2S formed in sulfide containing groundwater has been shown to partially passivate

the surface [80]. Additionally, cathodic stripping voltammetry at a potential of –1.1 V (SHE) in chloride solution with sulfide indicated the growth of a thick Cu_2S/Cu_2O outer layer in the was indicated by [47,80], with higher reduction charge linked to increased film thickness [80].

Our results support and expand upon previous findings by providing a more detailed insight through structural analysis. The observations confirm that sulfide-induced corrosion behavior is strongly influenced by the interaction between sulfide ions and the oxide film—particularly whether SH^- acts alone or in competition with dissolved O_2 with the concentration of sulfide ions also playing a key role in determining the nature of the resulting surface films [90].

4. Conclusions

The electrochemical properties, morphology and composition as well as thickness of corrosion layers of Cu and pre-oxidized copper in 0.2 M Cl^- with $5{\cdot}10^{-6}$ M SH^- or $1{\cdot}10^{-4}$ M SH^- were investigated at two temperatures, 22 °C and 60 °C in oxic conditions. The behavior of the copper and pre-oxidized copper was systematically evaluated through corrosion potential measurement during 24 h immersion in the solutions and the measurement of electrochemical impedance after the immersion, while the corrosion layers were analyzed using scanning electron microscopy, FIB-SEM, Raman analysis and cathodic stripping voltammetry. The aim of the study was to correlate the results with previous investigations and to evaluate the influence of the pre-oxidation of copper.

It was shown that the corrosion behavior of copper in saline environments with sulfides is dictated more by the structure and transport properties of its surface film than by equilibrium thermodynamics. Compact, p-type Cu_2O formed either naturally or by electrochemical pre-oxidation initially offers good protection, but its properties change by chloride and, more critically, by sulfide (SH^-) contamination.

Even though Cu_2O ($\Delta G^\circ = -141$ kJ mol^{-1}) is the thermodynamically preferred phase, sulfide ions accelerate transition to non-protective layer, converting protective oxide Cu_2O into a heterogeneous, defect-rich mixed Cu_2O/Cu_2S layer with high ionic transport properties. FIB-SEM cross-sections reveal that SH^- increases both porosity and total film thickness: from 75 to 120 nm in pure 0.2 M Cl^- to >500 nm and locally >2 μm, when $1{\cdot}10^{-4}$ M SH^- is present in chloride solution. The observed drop in charge-transfer resistance ($R_{ct} \approx 3$–5 kΩ cm^2) and rise in double-layer capacitance confirm that the mixed film no longer impedes corrosion.

Electrochemical pre-oxidation at −0.19 V generated a 15 nm Cu_2O layer that shifted initial E_{corr} to more positive values. After 24 h in chloride media, the film thickened, became porous with spatially separated n- and p-type regions, resulting in high ionic transport properties. In sulfide-contaminated solutions the pre-oxidized copper exhibited no superior corrosion resistance compared to bare copper, showing the important effect of film properties controlling protective performance.

At higher temperatures of 60 °C, film growth was faster, Cu_2S crystallized as needles or dense agglomerates, and hydrogen evolution at the Cu/film interface induced crack openings and local delamination. These observations highlight the synergistic impact of heat and sulfide on film destabilization.

CRediT authorship contribution statement

Klara Prijatelj: Writing – review & editing, Writing – original draft, Investigation, Formal analysis, Data curation, Conceptualization. **Tadeja Kosec:** Writing – review & editing, Writing – original draft, Supervision, Conceptualization.

Declaration of competing interest

The authors declare that they have no known competing financial interests or personal relationships that could have appeared to influence the work reported in this paper.

Acknowledgements

This work was fully financially supported by the Slovenian Research and Innovation Agency (ARIS) young research program within the program P2–0273. The help of Prof. Matjaž Finšgar for performing the XPS analysis, Dr. Barbara Šetina Batič for performing the SEM analysis, and Gregor Kapun for performing the FIB-SEM analysis is acknowledged and greatly appreciated.

Data availability

The research data is available at http://hdl.handle.net/20.500.12556/DiRROS-23268.

References

[1] X. Zhang, I. Odnevall Wallinder, C. Leygraf, Mechanistic studies of corrosion product flaking on copper and copper-based alloys in marine environments, Corros. Sci. 85 (2014) 15–25, https://doi.org/10.1016/j.corsci.2014.03.028.
[2] I. Odnevall Wallinder, X. Zhang, S. Goidanich, N.Le Bozec, G. Herting, C. Leygraf, Corrosion and runoff rates of Cu and three Cu-alloys in marine environments with increasing chloride deposition rate, Sci. Total Environ. 472 (2014) 681–694, https://doi.org/10.1016/j.scitotenv.2013.11.080.
[3] K. Rahmouni, M. Keddam, A. Srhiri, H. Takenouti, Corrosion of copper in 3% NaCl solution polluted by sulphide ions, Corros. Sci. 47 (2005) 3249–3266, https://doi.org/10.1016/j.corsci.2005.06.017.
[4] J. Becker, J. Pellé, S. Rioual, B. Lescop, N.Le Bozec, D. Thierry, Atmospheric corrosion of silver, copper and nickel exposed to hydrogen sulphide: a multi-analytical investigation approach, Corros. Sci. 209 (2022) 110726, https://doi.org/10.1016/j.corsci.2022.110726.
[5] C. Leygraf, I.O. Wallinder, J. Tidblad, T. Graedel, Atmospheric Corrosion, 1st ed, Wiley, 2016, pp. 290–301.
[6] D. Knotkova, K. Kreislova, Atmospheric corrosion and conservation of copper and bronze, in: A. Moncmanová (Ed.), Atmospheric corrosion and conservation of copper and bronze, WIT Transactions on State of the Art in Science and Engineering (2007) 107–142, https://doi.org/10.2495/978-1-84564-032-3/04.
[7] M. Reid, J. Punch, C. Ryan, L.F. Garfias, S. Belochapkine, J.P Franey, G.E. Derkits, W.D. Reents, Microstructural development of copper sulfide on copper exposed to humid H2S, J. Electrochem. Soc. 154 (2007) C209–C214.
[8] A.C. Nwanya, D. Obi, K.I. Ozoemena, R.U. Osuji, C. Awada, A. Ruediger, M. Maaza, F. Rosei, F.I. Ezema, Facile synthesis of nanosheet-like CuO film and its potential application as a high-performance pseudocapacitor electrode, Electrochim. Acta 198 (2016) 220–230, https://doi.org/10.1016/j.electacta.2016.03.064.
[9] X. Fuku, K. Kaviyarasu, N. Matinise, M. Maaza, Punicalagin green functionalized Cu/Cu2O/ZnO/CuO nanocomposite for potential electrochemical transducer and catalyst, Nanoscale Res. Lett. 11 (2016) 386, https://doi.org/10.1186/s11671-016-1581-8.
[10] S.S. Rathnakumar, K. Noluthando, A.J. Kulandaiswamy, J.B.B. Rayappan, K. Kasinathan, J. Kennedy, M. Maaza, Stalling behaviour of chloride ions: a non-enzymatic electrochemical detection of α-endosulfan using CuO interface, Sens. Actuators B: Chem. 293 (2019) 100–106, https://doi.org/10.1016/j.snb.2019.04.141.
[11] B.T. Sone, A. Diallo, X.G. Fuku, A. Gurib-Fakim, M. Maaza, Biosynthesized CuO nano-platelets: physical properties & enhanced thermal conductivity nanofluidics, Arab, J. Chem. 13 (2020) 160–170, https://doi.org/10.1016/j.arabjc.2017.03.004.
[12] J. Sackey, A.C. Nwanya, A.K.H. Bashir, N. Matinise, J.B. Ngilirabanga, A.E. Ameh, E. Coetsee, M. Maaza, Electrochemical properties of Euphorbia pulcherrima mediated copper oxide nanoparticles, Mater. Chem. Phys. 244 (2020) 122714, https://doi.org/10.1016/j.matchemphys.2020.122714.
[13] K. Ssekatawa, D.K. Byarugaba, M.K. Angwe, E.M. Wampande, F. Ejobi, E. Nxumalo, M. Maaza, J. Sackey, J.B. Kirabira, Phyto-mediated copper oxide nanoparticles for antibacterial, antioxidant and photocatalytic performances, Front. Bioeng. Biotechnol. 10 (2022) 820218, https://doi.org/10.3389/fbioe.2022.820218.
[14] P.A. Schweitzer, Atmospheric Degradation and Corrosion Control, Mercel Dekker, Inc, 1999 (n.d.).
[15] T. Kosec, J. Voglar, P. Močnik, A. Legat, Effect of the microstructural properties of copper on corrosion performance, Corros. Eng. Sci. Technol. 56 (2021) 728–735, https://doi.org/10.1080/1478422X.2021.1947942.
[16] A.H. Tuthill, Guidelines for the use of copper alloys ·in seawater, Mater. Perform. 26 (1987).
[17] N.W. Farro, L. Veleva, P. Aguilar, Copper marine corrosion: I. Corrosion rates in atmospheric and seawater environments of Peruvian port, TOCORRJ 2 (2009) 130–138, https://doi.org/10.2174/1876503300902010130.
[18] L. Robbiola, J.-M. Blengino, C. Fiaud, Morphology and mechanisms of formation of natural patinas on archeological Cu-Sn alloys, Corros. Sci. 12 (1998) 2083–2111.
[19] J. Kruger, The Oxide Films Formed on Copper Single Crystal Surfaces in Water, 108 National Bureau of Standards, Washington, D. C, 1961.
[20] B.C. Syrett, S.S. Wing, D.D. MacDonald, A Study to Determine the Mechanisms of Corrosion of Copper-Nickel Alloys in Sulfide-Polluted Seawater (Report No. ADA051833), Defense Technical Information Center, Fort Belvoir, VA, 1979, https://doi.org/10.21236/ADA066257.

[21] S.B. Adeloju, Y.Y. Duan, Corrosion resistance of Cu2O and CuO on copper surfaces in aqueous media, Br. Corros. J. (1994) 309–314, https://doi.org/10.1179/000705994798267485.
[22] R.F. North, M.J. Pryor, The influence of corrosion product structure on the corrosion rate of Cu-Ni alloys, Corros. Sci. (1970) 297–311, https://doi.org/10.1016/S0010-938X(70)80022-1.
[23] G. Kear, B.D. Barker, F.C. Walsh, Electrochemical corrosion of unalloyed copper in chloride media—a critical review, Corros. Sci. 46 (2004) 109–135, https://doi.org/10.1016/S0010-938X(02)00257-3.
[24] A. Srivastava, R. Balasubramaniam, Electrochemical impedance spectroscopy study of surface films formed on copper in aqueous environments, Mater. Corros. 56 (2005) 611–618, https://doi.org/10.1002/maco.200503866.
[25] F. King, C. Lilja, K. Pedersen, P. Pitkänen, M. Vähänen, An update of the state-of-the-art report on the corrosion of copper under expected conditions in a deep geologic repository, in: Technical report TR-10-67, Svensk Kärnbränslehanttering AB, Stockholm, 2010.
[26] A. El Warraky, H.A. El Shayeb, E.M. Sherif, Pitting corrosion of copper in chloride solutions, Anti-Corros. Methods Mater. 51 (2004) 52–61, https://doi.org/10.1108/00035590410512735.
[27] K. Liang, Y. Xu, Q. Lu, S. Zhang, Y. Tan, Investigation of copper corrosion behavior in various sulfide solutions, in: Proceedings of the 2017 International Conference on Material Science, Energy and Environmental Engineering (MSEEE 2017), Atlantis Press, Xi'an, China, 2017, https://doi.org/10.2991/mseee-17.2017.78.
[28] L.E. Eiselstein, B.C. Syrett, S.S. Wing, R.D. Caligiuri, The accelerated corrosion of Cu Ni alloys in sulphide-polluted seawater: mechanism no. 2, Corros. Sci. 23 (1983) 223–239, https://doi.org/10.1016/0010-938X(83)90104-X.
[29] E.D. Mor, A.M. Beccaria, G. Poggi, Behaviour of zinc in sea water in the presence of sulphides, Br. Corros. J. 9 (1974) 53–56, https://doi.org/10.1179/000705974798321684.
[30] J.N. Al-Hajji, M.R. Reda, The corrosion of copper-nickel alloys in sulfide-polluted seawater: the effect of sulfide concentration, Corros. Sci. 34 (1993) 163–177, https://doi.org/10.1016/0010-938X(93)90266-J.
[31] D.D. Macdonald, B.C. Syrett, S.S. Wing, The corrosion of copper-nickel alloys 706 and 715 in flowing sea water. I-effect of oxygen, Corrosion 34 (1978) 289–301, https://doi.org/10.5006/0010-9312-34.9.289.
[32] A.M.Y. Taher, Corrosion behavior of copper-nickel alloy in marine environment (Review Paper), AMM 799–800 (2015) 222–231. https://doi.org/10.4028/www.scientific.net/AMM.799-800.222.
[33] K. Gong, C. Zheng, D. Zhang, T. Lv, X. Ju, Study on seawater corrosion resistance of copper alloy, J. Phys.: Conf. Ser. 2783 (2024) 012060, https://doi.org/10.1088/1742-6596/2783/1/012060.
[34] G. Li, H. Xing, M. Du, M. Sun, L. Ma, Accelerated corrosion of 70/30 copper-nickel alloys in sulfide-polluted seawater environment by sulfide, J. Mater. Res. Technol. 30 (2024) 8620–8634, https://doi.org/10.1016/j.jmrt.2024.05.212.
[35] F.M. Al Kharafi, I.M. Ghayad, B.G. Ateya, Rapid intergranular corrosion of copper in sulfide-polluted salt water, Electrochem. Solid-State Lett. 11 (2008), https://doi.org/10.1149/1.2832428. G15.
[36] J. Halldin Stenlid, E. Campos dos Santos, A.J. Johansson, L.G.M. Pettersson, Properties of interfaces between copper and copper sulphide/oxide films, Corros. Sci. 183 (2021) 109313, https://doi.org/10.1016/j.corsci.2021.109313.
[37] B. Valdez Salas, M. Schorr Wiener, R. Zlatev Koytchev, G. López Badilla, R. Ramos Irigoyen, M. Carrillo Beltrán, N. Radnev Nedev, M. Curiel Alvarez, N. Rosas Gonzalez, J.M. Bastidas Rull, Copper corrosion by atmospheric pollutants in the electronics industry, ISRN Corrosion (2013) 1–7, https://doi.org/10.1155/2013/846405, 2013.
[38] E. Salahinejad, R. Eslami-Farsani, L. Tayebi, Corrosion failure analysis of printed circuit boards exposed to H2S-containing humid environments, Eng. Fail. Anal. 79 (2017) 538–546, https://doi.org/10.1016/j.engfailanal.2017.05.038.
[39] M.B. McNeil, A.L. Amos, T.L. Woods, ***Technical note:*** adherence of sulfide mineral layers produced by corrosion of copper alloys, Corrosion 49 (1993) 755–758. https://doi.org/10.5006/1.3316128.
[40] M.A. Javed, W.C. Neil, Microbiologically influenced corrosion of copper and its alloys - a review, Corros. Prev. Control. (2016) 1–14.
[41] D.S. Hall, M. Behazin, W.Jeffrey Binns, P.G. Keech, An evaluation of corrosion processes affecting copper-coated nuclear waste containers in a deep geological repository, Prog. Mater. Sci. 118 (2021) 100766, https://doi.org/10.1016/j.pmatsci.2020.100766.
[42] A.J. Johansson, D. Svensson, A. Gordon, H. Pahverk, O. Karlsson, J. Brask, M. Lundholm, D. Malmström, F. Gustavsson, Corrosion of copper after 20 years exposure in the bentonite field tests LOT S2 and A3, in: Technical report TR-20-14, Svensk Kärnbränslehanttering AB, Stockholm, 2020.
[43] J. McMurry, B.M. Ikeda, S. Stroes-Gascoyne, D.A. Dixon, Evaluation of canadian deep geological repository: defective container scenario, in: Report No: 06819-REP-01200-10127-R00, Atomic Energy of Canada Limited, 2004.
[44] L. Duro, E. Colàs, V. Montoya, D.G. Cobos, Groundwater equilibration and radionuclide solubility calculations, NWMO TR-2010-02 (2010).
[45] E. Salehi Alaei, M. Guo, J. Chen, M. Behazin, E. Bergendal, C. Lilja, D. W. Shoesmith, J.J. Noël, The transition from used fuel container corrosion under oxic conditions to corrosion in an anoxic environment, Mater. Corros. (2023), https://doi.org/10.1002/maco.202313757 maco.202313757.
[46] J. Chen, X. Pan, T. Martino, C. Lilja, M. Behazin, W.J. Binns, P.G. Keech, J.J. Noël, D.W. Shoesmith, The effects of chloride and sulphate on the growth of sulphide films on copper in anoxic sulphide solutions, Mater. Corros. 74 (2023) 1665–1676, https://doi.org/10.1002/maco.202313766.
[47] J. Smith, Z. Qin, F. King, L. Werme, D.W. Shoesmith, Sulfide film formation on copper under electrochemical and natural corrosion conditions, Corrosion 63 (2007) 135–144, https://doi.org/10.5006/1.3278338.
[48] H.M. Hollmark, P.G. Keech, J.R. Vegelius, L. Werme, L.-C. Duda, X-ray absorption spectroscopy of electrochemically oxidized Cu exposed to Na2S, Corros. Sci. 54 (2012) 85–89, https://doi.org/10.1016/j.corsci.2011.09.001.
[49] M. Bojinov, S. Goel, T. Ikäläinen, T. Saario, Effect of sulfide addition on the corrosion mechanism of copper in saline groundwater solution, J. Electrochem. Soc. 171 (2024) 041505, https://doi.org/10.1149/1945-7111/ad3fed.
[50] V. Ratia-Hanby, E. Isotahdon, X. Yue, P. Malmberg, C. Leygraf, J. Pan, E. Huttunen-Saarivirta, Characterization of surface films that develop on pre-oxidized copper in anoxic simulated groundwater with sulphide, Colloids Surf. 676 (2023) 132214, https://doi.org/10.1016/j.colsurfa.2023.132214.
[51] T. Martino, J. Smith, J. Chen, Z. Qin, J.J. Noël, D.W. Shoesmith, The properties of electrochemically-grown copper sulfide films, J. Electrochem. Soc. 166 (2019) C9–C18, https://doi.org/10.1149/2.0321902jes.
[52] D.C. Harris, Quantitative Chemical Analysis, 2007, 7. ed., 2. print.
[53] H.-D. Speckmann, M.M. Lohrengel, J.W. Schultze, H.-H. Strehblow, The growth and reduction of duplex oxide films on copper, Ber.Bunsen-Ges Phys. Chem. 89 (1985) 392–402, https://doi.org/10.1002/bbpc.19850890408.
[54] R. Babić, M. Metikoš-Huković, A. Jukić, A study of copper passivity by electrochemical impedance spectroscopy, J. Electrochem. Soc. 148 (2001) B146, https://doi.org/10.1149/1.1354608.
[55] R.A. Robie, P.M. Bethke, * Molar volumes and densities of minerals, U.S. Geological Survey (1962), https://doi.org/10.3133/70159012 n.d.
[56] D.A. Shirley, High-resolution X-ray photoemission spectrum of the valence bands of gold, Phys. Rev. B 5 (1972) 4709–4714, https://doi.org/10.1103/PhysRevB.5.4709.
[57] L.M. Abrantes, L.M. Castillo, C. Norman, L.M. Peter, A photoelectrochemical study of the oxidation of copper in alkaline solution, J. Electroanal. Chem. 163 (1984) 209–221, https://doi.org/10.1016/S0022-0728(84)80053-4.
[58] H.-H. Strehblow, V. Maurice, P. Marcus, Initial and later stages of anodic oxide formation on Cu, chemical aspects, structure and electronic properties, Electrochim. Acta 46 (2001) 3755–3766, https://doi.org/10.1016/S0013-4686(01)00657-0.
[59] J.M. Smith, J.C. Wren, M. Odziemkowski, D.W. Shoesmith, The electrochemical response of preoxidized copper in aqueous sulfide solutions, J. Electrochem. Soc. 154 (2007) C431, https://doi.org/10.1149/1.2745647.
[60] M.R.G. De Chialvo, S.L. Marchiano, A.J. Arvía, The mechanism of oxidation of copper in alkaline solutions, J. Appl. Electrochem. 14 (1984) 165–175, https://doi.org/10.1007/BF00618735.
[61] M. Seo, X.C. Jiang, N. Sato, Photoacoustic study on cathodic reduction of anodic oxide films formed on copper in borate solution, Mater. Corros. 39 (1988) 583–588, https://doi.org/10.1002/maco.19880391205.
[62] I. Milošev, H.-H. Strehblow, Electrochemical behavior of Cu-xZn alloys in borate buffer solution at pH 9.2, J. Electrochem. Soc. 150 (2003) B517, https://doi.org/10.1149/1.1615997.
[63] Y.-Y. Su, S. Nakayama, T. Osakai, Cathodic reduction of copper oxides, Corrosion Reviews 29 (2011), https://doi.org/10.1515/corrrev.2011.001.
[64] F. Ammeloot, B. Millet, C. Fiaud, L. Robbiola, E. Sutter, Characterization of naturally grown oxide layers on copper with and without benzotriazole by electrochemical and photoelectrochemical measurements, METAL 59, in: International conference on metals conservation, Semur-en-Auxois, France, Sep 1995, pp. 109–117, hal-00975720.
[65] J.-Z. Zhang, F.J. Millero, The products from the oxidation of H2S in seawater, Geochimica et Cosmochim. Acta 57 (1993) 1705–1718, https://doi.org/10.1016/0016-7037(93)90108-9.
[66] Ö.H. Göte, J. Alexander, Oxidation rate of sulfide in sea water, A preliminary study, J. Geophys. Res. 68 (1963) 3995–3997, https://doi.org/10.1029/JZ068i013p03995.
[67] B.C. Syrett, The mechanism of accelerated corrosion of copper-nickel alloys in sulphide-polluted seawater, Corros. Sci. 21 (1981) 187–209, https://doi.org/10.1016/0010-938X(81)90030-5.
[68] I.D. Raistrick, J.R. MacDonald, D.R. Franceschetti, Impedance Spectroscopy Emphasizing Solid Materials and Systems, John Wiley&Sons, New York, 1987, pp. 87–99.
[69] G.J. Brug, The analysis of electrode impedances complicated by the presence of a constant phase element, J. Electroanal. Chem. 176 (1984) 275–295.
[70] L. Pauling, in: W.H. Freeman (Ed.), General Chemistry, 3d ed, 1970.
[71] T. Martino, J. Chen, J.J. Noël, D.W. Shoesmith, The effect of anions on the anodic formation of copper sulphide films on copper, Electrochim. Acta 331 (2020) 135319, https://doi.org/10.1016/j.electacta.2019.135319.
[72] Y. Deng, A.D. Handoko, Y. Du, S. Xi, B.S. Yeo, In situ raman spectroscopy of copper and copper oxide surfaces during electrochemical oxygen evolution reaction: identification of Cu ^{III} oxides as catalytically active species, ACS Catal 6 (2016) 2473–2481, https://doi.org/10.1021/acscatal.6b00205.
[73] H.Y.H. Chan, C.G. Takoudis, M.J. Weaver, Oxide film formation and oxygen adsorption on copper in aqueous Media As probed by surface-enhanced raman spectroscopy, J. Phys. Chem. B 103 (1999) 357–365, https://doi.org/10.1021/jp983787c.
[74] A. Kudelski, B. Pettinger, Raman study on methanol partial oxidation and oxidative steam reforming over copper, Surf. Sci. 566–568 (2004) 1007–1011, https://doi.org/10.1016/j.susc.2004.06.046.
[75] L.I. McCann, K. Trentelman, T. Possley, B. Golding, Corrosion of ancient Chinese bronze money trees studied by Raman microscopy, J. Raman Spectrosc. 30 (1999)

121–132, https://doi.org/10.1002/(SICI)1097-4555(199902)30:2<121::AID−JRS355>3.0.CO;2-L.
[76] T. Kosec, M.B. Leban, P. Ropret, M. Finšgar, The impact of urban rain on the changes of bare and artificially patinated bronze during 9-year exposure, Environ. Sci. Pollut. Res. (2024), https://doi.org/10.1007/s11356-024-33369-9.
[77] Database of raman spectroscopy, X-ray diffraction and chemistry of minerals, (n. d.). https://rruff.info/(accessed December 29, 2024).
[78] G.G. Welegergs, N. Numan, S. Dube, Z. Nuru, N. Botha, K. Cloete, S. Azizi, I. Madiba, M. Akbari, M. Tsegay, H. Gebretinsae, C. Mtshali, Z. Khumalo, F. Ezema, A. Krief, A. Gibaud, M. Henini, M.P. Seopela, M. Chaker, M. Maaza, Room temperature surface bio-sulfurisation via natural Sativum annilin and bioengineering of nanostructured CuS/Cu 2S, Nano-Horizons 2 (2023), https://doi.org/10.25159/NanoHorizons.45486dad4f94.
[79] M. Guo, J. Chen, T. Martino, M. Biesinger, J.J. Noël, D.W. Shoesmith, The susceptibility of copper to pitting corrosion in borate-buffered aqueous solutions containing chloride and sulfide, J. Electrochem. Soc. 166 (2019) C550–C558, https://doi.org/10.1149/2.0611915jes.
[80] T. Kosec, Z. Qin, J. Chen, A. Legat, D.W. Shoesmith, Copper corrosion in bentonite/saline groundwater solution: effects of solution and bentonite chemistry, Corros. Sci. 90 (2015) 248–258, https://doi.org/10.1016/j.corsci.2014.10.017.
[81] J. Rumble, CRC Handbook of Chemistry and Physics, 106th, 2025.
[82] J.H. Payer, G. Ball, B.I. Rickett, H.S. Kim, Role of transport properties in corrosion product growth, Mater. Sci. Eng. A 198 (1995) 91–102, https://doi.org/10.1016/0921-5093(95)80063-Z.
[83] B. Millet, C. Fiaud, C. Hinnen, E.M.M. Sutter, A correlation between electrochemical behaviour, composition and semiconducting properties of naturally grown oxide films on copper, Corrosi. Sci. 37 (1995) 1903–1918, https://doi.org/10.1016/0010-938X(95)00072-R.
[84] T. Martino, R. Partovi-Nia, J. Chen, Z. Qin, D.W. Shoesmith, Mechanisms of film growth on copper in aqueous solutions containing sulphide and chloride under voltammetric conditions, Electrochim. Acta 127 (2014) 439–447, https://doi.org/10.1016/j.electacta.2014.02.050.
[85] J. Chen, Z. Qin, T. Martino, D.W. Shoesmith, Non-uniform film growth and micro/macro-galvanic corrosion of copper in aqueous sulphide solutions containing chloride, Corros. Sci. 114 (2017) 72–78, https://doi.org/10.1016/j.corsci.2016.10.024.
[86] J. Chen, Z. Qin, L. Wu, J.J. Noël, D.W. Shoesmith, The influence of sulphide transport on the growth and properties of copper sulphide films on copper, Corros. Sci. 87 (2014) 233–238, https://doi.org/10.1016/j.corsci.2014.06.027.
[87] U. Collisi, H.-H. Strehblow, The formation of Cu2O layers on Cu and their electrochemical and photoelectrochemical properties, J. Electroanal. Chem. Interfacial Electrochem. 284 (1990) 385–401, https://doi.org/10.1016/0022-0728(90)85046-8.
[88] J. Chen, Z. Qin, T. Martino, M. Guo, D.W. Shoesmith, Copper transport and sulphide sequestration during copper corrosion in anaerobic aqueous sulphide solutions, Corros. Sci. 131 (2018) 245–251, https://doi.org/10.1016/j.corsci.2017.11.025.
[89] M.R. Reda, J.N. Alhajji, Deleterious role of complexing agents in corrosion of copper-nickel alloys in sulphide polluted sea water, B. Corros. J. 30 (1995) 56–62, https://doi.org/10.1179/bcj.1995.30.1.56.
[90] F.M. Al Kharafi, A.M. Abdullah, I.M. Ghayad, B.G. Ateya, Effect of sulfide pollution on the stability of the protective film of benzotriazole on copper, Appl. Surf. Sci. 253 (2007) 8986–8991, https://doi.org/10.1016/j.apsusc.2007.05.017.